Peculiarities of Photoinduced Electron Transfer in Nanoassemblies Containing Porphyrin Macrocycles

Eduard I. Zenkevich,[a,b@] and Christian von Borczyskowski[c]

[a]*Belarussian National Technical University, 220013 Minsk, Belarus*
[b]*Chemnitz University of Technology, Research Center for Materials, Architectures and Integration of Nanomembranes (MAIN), 09107 Chemnitz, Germany*
[c]*Institute of Physics, Chemnitz University of Technology, 09107 Chemnitz, Germany*
[@]*Corresponding author E-mail: zenkev@tut.by*

Dedicated to the blessed memory of our colleague Academician O. I. Koifman

Using the combination of spectral static and time-resolved experimental data together with theoretical calculations in the frames of the corresponding models, the dynamics of competing non-radiative relaxation processes was quantitatively studied for various nanoassemblies containing porphyrin macrocycles (meso-nitrophenyloctaethylporphyrins and their chemical dimers; Zn-porphyrin chemical dimers covalently linked with electron acceptor of non-porphyrin nature; self-assembled porphyrin triads with covalently linked electron acceptors) upon variation of properties of surrounding. Especial attention was paid to the analysis of some peculiarities of the photoinduced electron transfer (PET) in few unusual and rare cases: i) the direct PET "through-space" mechanism with participation of S_1 and T_1 states in the conditions of strong steric interactions between bulky C_2H_5 substituents in β-positions of pyrrole rings and NO_2 group; ii) the competition of PET and energy migration in Zn-porphyrin chemical dimers with covalently linked electron acceptor; iii) in self-assembled porphyrin triads, the extra-ligand S_1 state quenching via hole transfer "extra-ligand $\rightarrow$ dimer" followed by the efficient formation of the locally excited T_1 state of porphyrin free base; iv) realization of low-temperature PET in triads containing fluorinated porphyrin as electron acceptor; v) the extra-ligand S_1 state quenching via long-range superexchange PET to covalently linked electron acceptor in triads.

Keywords: Porphyrin supramolecular complexes, S_1 and T_1 state quenching, picosecond and femtosecond time-resolved spectroscopy, donor-acceptor interactions, photoinduced electron transfer, energy migration, sterically hindered effects and non-planar conformations, Marcus theory, superexchange electron transfer.

Особенности фотоиндуцированного переноса электрона в наноансамблях, содержащих порфириновые макроциклы

Э. И. Зенькевич,[a,b@] К. фон Борцисковски[c]

[a]*Белорусский национальный технический университет, 220013 Минск, Беларусь*
[b]*Технический университет Хемница, Центр исследования материалов, архитектур и интегрирования наномембран (МАИН), D-09107 Хемниц, Германия*
[c]*Институт физики, Технический университет Хемница, D-09107 Хемниц, Германия*
[@]*E-mail: zenkev@tut.by*

С использованием комбинации спектральных стационарных и время-разрешенных экспериментальных данных совместно с теоретическими расчетами в рамках соответствующих моделей количественно исследована динамика конкурирующих безызлучательных релаксационных процессов для различных наноансамблей, содержащих порфириновые макроциклы (мезо-нитрофенилоктаэтилпорфирины и их химические димеры; химические димеры Zn-порфиринов, ковалентно связанные с электронными акцепторами непорфириновой природы; самособирающиеся триады порфиринов с ковалентно связанными акцепторами электрона) при вариации свойств окружения. Особое внимание уделяется анализу некоторых особенностей фотоиндуцированного переноса электрона (PET) в нескольких необычных и редких случаях: i) прямой меха-

низм пространственного PET с участием S_1 и T_1 состояний в условиях сильных стерических взаимодействий между NO_2 группой и объемными C_2H_5 заместителями в β-положениях пиррольных колец; ii) конкуренция PET и миграции энергии в химических димерах Zn-порфирина с ковалентно связанным акцептором электрона; iii) тушение S_1 состояния экстра-лиганда в самособирающихся триадах порфиринов в результате переноса дырки «экстра-лиганд → димер», сопровождающегося эффективным заселением локально возбужденного T_1 состояния свободного основания порфирина; iv) реализация низкотемпературного PET в триадах, содержащих фторированный порфирин в качестве акцептора электрона; v) тушение S_1 состояния экстра-лиганда за счет дистанционного PET по механизму суперобмена на ковалентно-связанный акцептор электрона в триадах.

Ключевые слова: Порфириновые супрамолекулярные комплексы, тушение S_1 и T_1 состояний, пикосекундная и фемтосекундная время-разрешенная спектроскопия, донорно-акцепторные взаимодействия, фотоиндуцированный перенос электрона, перенос энергии, стерически напряженные порфирины и неплоские конформации, теория Маркуса, перенос электрона по механизму суперобмена.

Introduction

Today it is well documented that tetrapyrrole macrocycles displaying an impressive variety of electronic and optical properties, connected partly with various central metals, are considered as pigments of life in nature, performing different functions in living systems depending on the bound metal ion.[1] Magnesium containing chlorophylls and bacteriochlorophylls are the vital chromophores embedded in the light-harvesting complexes and reaction centers of the photosynthetic units of plants, algae, mosses and bacteria; iron containing heme is responsible for oxygen transport and electron transfer in blood; cobalt and nickel containing porphyrins act as vitamins or promote bacterial methane metabolism. Thus, it's not surprising that a huge range of tetrapyrrole compounds as well multi-porphyrin arrays has been investigated, with the goal of synthetizing efficient bioinspired molecular systems for light harvesting (energy transfer events), charge separation (photoinduced electron/hole transfer), photocatalytic processes, nanoelectronics and biomedicine.[2-18] It was evidently shown that self-assembly is promising for construction of a wide variety of multiporphyrin nano-assemblies, whose 1D/2D/3D structures are typically relevant to their functions. In-depth understanding of their structure-function correlations is essential for rational design and development of functional multiporphyrin nano-assemblies.[19] Given the potential applications and the need for better theoretical frameworks, the design and construction of novel multiporphyrin architectures by self-assembly and self-organization continues to be an active research area.

In this respect without any doubts, Ivanovo team (Ivanovo State University of Chemical Technology, Russia) under leadership of full member of Russian Academy of Sciences Professor Oskar I. Koifman (and his teacher Professor Boris D. Berezin in former times) is known in the world scientific community, and has succeeded a lot of principal results in porphyrin related directions including synthetic strategy, physical and coordination chemistry of tetrapyrrolic macrocycles, construction and study of supramolecular assemblies on their basis as well as realization of various practical applications in industrial chemistry, catalysis and biomedicine. Academician O.I. Koifman published more than 1360 scientific works, including 9 monographs, 18 chapters in monographs, 22 review articles, and 80 inventor's certificates and patents as well as was a supervisor of 8 doctoral dissertations and 27 PhD dissertations. From our side, with his participation we have successfully realized the International INTAS project (2004-2008) and two Russian-Belarussian projects (2014-2016, 2018-2020). In fact, Prof. Koifman has gained the respect of the scientific community and the broader community engaged in science policy work, both nationally and internationally, due to his outstanding scientific accomplishments, his support of a young generation of scientists, and the leadership and vision he has displayed. With profound sadness we knew the passing of Prof. Oskar Koifman on December 31st, 2023. For all of us who have had the privilege of knowing him — whether as friends, colleagues, collaborators, or students — it is an immense fortune to get acquainted with Prof. Koifman and have opportunities to know his intelligence, high scientific level and warmth firsthand.

Concerning the nature of the non-radiative channels of excitation energy relaxation in multiporphyrin nano-assemblies of various composition and morphology one should mention the following. From photophysical background, the observed luminescence quenching of some components in multiporphyrin complexes may be interpreted as being due to Förster inductive-resonance energy transfer (FRET)[20,21] and/or the photoinduced charge (electron or hole) transfer.[22-24] In this respect, one principle remark should be underline: according to classical Marcus theory[22] in case of charge transfer process the emission of both donor and acceptor of charge is supposed to be quenched in more or less extent (see Figure 1).

By now, taking into account this aspect various systems with two or more identical tetrapyrrolic donors or acceptors have been studied using noncovalent D/A mixtures and assemblies, as well as covalent D−A porphyrin dyads and triads with electron acceptors of the non-porphyrin nature, all of which have the potential for electron/hole hopping or delocalization between the two A or D species.[25-35]
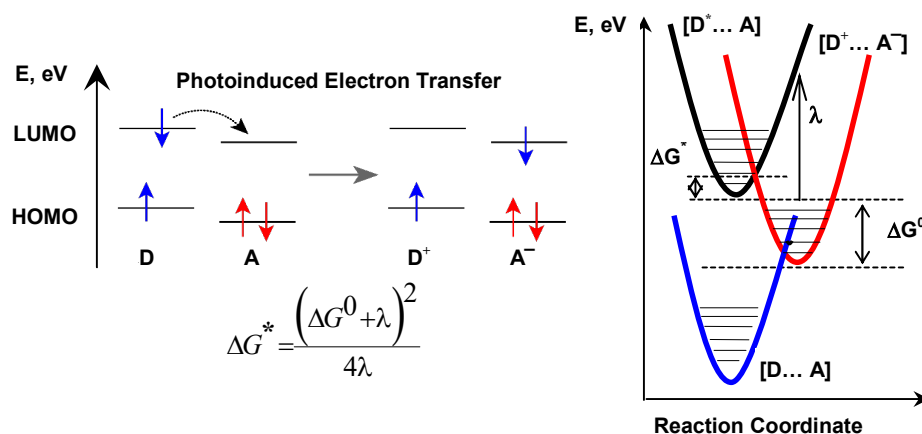
Figure 1. Processes and energetic scheme of non-adiabatic endergonic photoinduced electron transfer in the "normal" region according to classical Marcus theory.[22] Physico-chemical meaning of abbreviations included in the formula will be given in the text.

Here, in this semi-review paper, taking into account our recent results (including experimental findings and theoretical calculations, which have been obtained partly with participation of representatives of Ivanovo team) we would like to present quantitative comprehensive analysis of the reasons of luminescence quenching due to competing non-radiative relaxation processes paying an especial attention to the analysis of some peculiarities of photoinduced electron transfer (PET) presumably. Moreover, we would like to analyze few unusual and relatively rare cases: i) the direct PET "through-space" mechanism in porphyrin macrocycles with participation of S_1 and T_1 states in the conditions of strong steric interactions between bulky C_2H_5 substituents in β-positions of pyrrole rings and NO_2 group; ii) the competition of PET and energy migration in Zn-porphyrin chemical dimers with covalently linked electron acceptor; iii) the extra-ligand S_1 state quenching via hole transfer "extra-ligand → dimer" followed by the efficient formation of the locally excited T_1 state of porphyrin free base in self-assembled porphyrin triads; iv) realization of low-temperature PET in triads containing fluorinated porphyrin as electron acceptor; v) the extra-ligand S_1 state quenching via long-range superexchange PET in porphyrin triads containing covalently linked electron acceptor of non-porphyrin nature. Correspondingly, a comparative and

quantitative description of these rare PET phenomena in nanoassemblies of various morphology containing tetrapyrrolic subunits may be considered as a main goal of this contribution.

Experimental

Synthesis, purification and characterization of 5-(*ortho*-methylphenyl)- and 5-(*ortho*-nitrophenyl)-2,3,7,8,12,13,17,18-octaethylporphyrins (OEP-Ph(*o*-CH₃) and OEP-Ph(*o*-NO₂)), and their palladium(II) complexes (PdOEP-Ph(*o*-CH₃) and PdOEP-Ph(*o*-NO₂)) were performed by Dr. A. Shulga and described in our earlier publications[36-38] (Figure 2A). The octaethylporphyrin chemical dimers with *meso*-phenyl spacer OEP-Ph-OEP as well as their *meso*-nitrophenyl substituted derivatives OEP-Ph-OEP-Ph(*o*-NO₂) were synthesized according to the known methods[39-40] (Figure 2B).

The preparation, identification and purification of the chemical dimer (ZnOEP)₂Ph with *meso*-phenyl spacer was reported by us earlier.[39] The corresponding compounds based on the dimer (ZnOEP)₂Ph and electron acceptors *para*-benzoquinone (Q) and pyromellitimide (Pim) were prepared and identified according to known procedures.[41] Pim was comparatively used because of the simple detection of the characteristic absorption band of its anion radical (λ_{max}=715 nm [42]) and a pertinent one-electron reduction potential with respect to the chemical dimer (ZnOEP)₂Ph. The corresponding structures are shown in Figure 3.
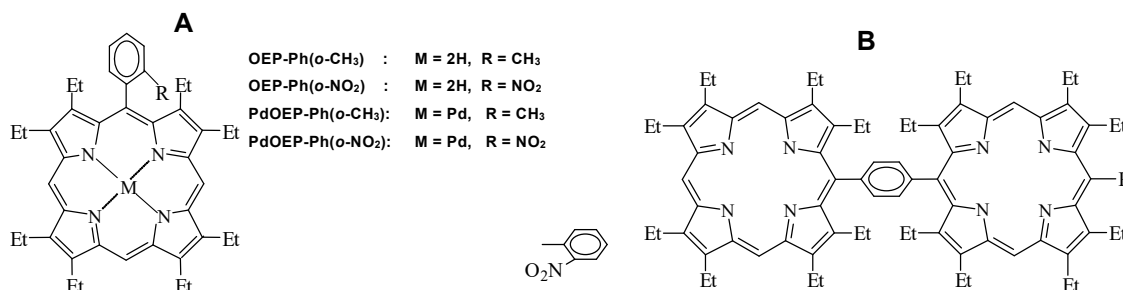

Figure 2. Structures and abbreviations of *meso*-nitrophenyl and methylphenyl substituted octaethylporphyrins, and the corresponding Pd-complexes (**A**), as well as their chemical dimers (**B**).

A₁: *para*-benzoquinone (Q)
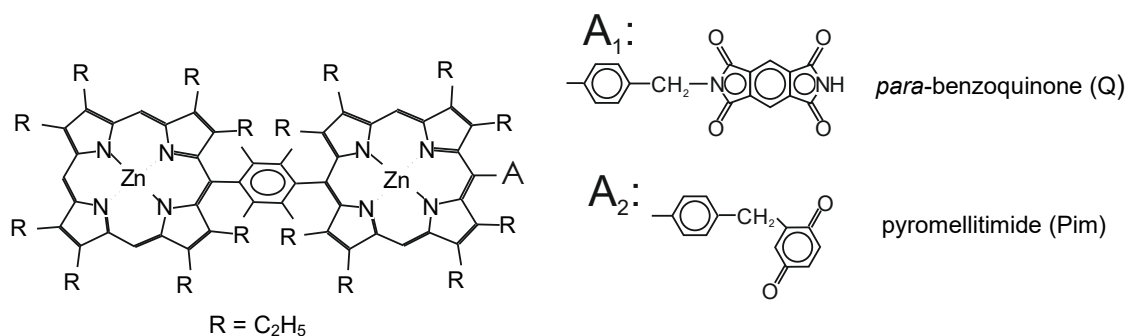
A₂: pyromellitimide (Pim)

R = C₂H₅

Figure 3. Structures and abbreviations of chemical dimer (ZnOEP)₂Ph with *meso*-phenyl spacer as well its derivatives containing electron acceptors *para*-benzoquinone(Q) and pyromellitimide (Pim) covalently linked via *meso*-phenyl ring to the dimer.
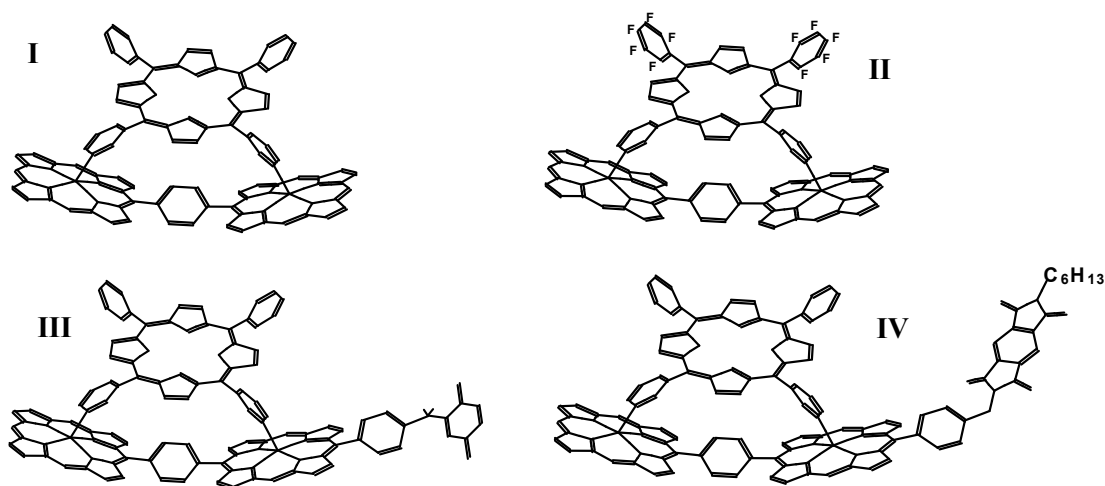

Figure 4. Mutual arrangement of the chemical dimer (ZnOEP)₂Ph and porphyrin extra-ligands in triads without electron acceptor (**I, II**) and triads containing electron acceptors, quinone Q and piromellitimide Pim, covalently linked to the dimer (**III, IV**). **I**: (ZnOEP)₂Ph⊗ H₂P(m^Pyr)₂-(iso-PrPh)₂; **II**: (ZnOEP)₂Ph⊗H₂P(m^Pyr)₂-(5FPh)₂; **III**: (ZnOEP)₂Ph-Q⊗H₂P(m^Pyr)₂-(iso-PrPh)₂; **IV**: (ZnOEP)₂Ph-Pim⊗H₂P(m^Pyr)₂-(iso-PrPh)₂. Optimized geometries have been calculated on the basis of HyperChem software package (release 4, semiempirical method PM3). For clarity, side alkyl substituents in pyrrole rings of the dimer and *meso*-phenyl rings of the extra-ligand are omitted. Central Zn ions in the dimer are coupled by co-ordination bonds with nitrogens of pyridyl rings (Pyr) of tetrapyrrole extra-ligands (H₂P is porphyrin). Two-fold interaction is formed via adjacent (^) pyridyl rings having nitrogens in *meta*- (m) positions. The symbol ⊗ is used in order to show what interacting subunits (dimer and extra-ligand) are bound together.

Self-assembled porphyrin triads of various but controlable geometry were formed (using the extra-ligation effect[39]) during a successive titration of the dimer (ZnOEP)₂Ph solution with dipyridyl-substituted porphyrin free base (H₂P) and its pentafluorinated derivative (H₂PF) described in our publications.[10,11,39,43] Two types of the triads with the same geometry and the same dimer will be discussed in this paper: one type contains usual porphyrin extra-ligand H₂P(m^Pyr)₂-(iso-PrPh)₂ with adjacent pyridyl rings or its fluorinated derivative 5,10-di(penta-fluorophenyl)-15,20-dipyridyl free base porphyrin, H₂P(m^Pyr)₂-(5FPh)₂ known as a strong electron acceptor.[10,27,43] In the triads of the other type, the chemical dimer (ZnOEP)₂Ph additionally is covalently linked in *meso*-position to an electron acceptors, such as *para*-benzoquinone (Q) or pyromellitimide (Pim). For such triads, we like to discuss some aspects of interporphyrin and porphyrin→quinone PET events competing with the non-radiative energy transfer processes. The structures of the corresponding self-assembled triads of both types are shown in Figure 4.

The static fluorescence and excitation spectra were recorded on a Shimadzu RF-5001PC spectrofluorometer and absorption spectra on a Shimadzu UV-3101PC spectrophotometer. For temperature dependent measurements a homemade cryostat was used. They served as an experimental background showing the stability of the objects under study, their spectral properties and the self-assembly of the triads. The most principal findings showing the interactions of the counterparts as well as the temporal dynamics of the excited states for subunits were obtained on the basis of time resolved fluorescence and transient pump-probe results using the corresponding home-made equipment described in[11,28,43] (Figure 5).

Picosecond time-resolved fluorescence measurements (the time correlated single photon counting, TCSPC experiments) were performed out using laser picosecond fluorescent setup with 2-D (wavelength-time) registration based on a dye laser (repetition rate 4 MHz, 10 ps pulses) and a Streak-Scope (Hamamatsu Model C4334, experimental response Δ₁/₂ ≈30 ps). Pump-probe experiments involved a Coherent MIRA 900 Ti:sapphire laser with a regenerative amplifier and a parametric oscillator running at 1 kHz. Excitation in the 400-800 nm range was used, the experimental response was Δ₁/₂ ≈ 120 fs. For temperature dependent measurements a homemade cryostat was used equipped with the temperature controller ITC502 (Oxford Instruments).

Results and Discussion

1. Influence of steric hindrance interactions on photoinduced electron transfer in meso-nitrophenyl-octaethylporphyrins and their chemical dimers

Previously, we have shown for the first time[10,36,37,44] that in OEP-(Ph) molecule as well as in its Zn- and Pd-complexes, one *meso*-phenyl substitution leads to steric interactions of *meso*-phenyl ring with bulky β-alkyl substituents followed by the non-planar deformations of the porphyrin macrocycle in the T_1 state presumably what manifests itself in the strong decay shortening (by ~ 300 times) of T_1 state while properties of S_1 state remain unchanged practically. In addition, it was shown within fruitful cooperation with Ivanovo team[45-49] as well as by other groups[50-55] that with increasing the number (n = 1÷4) of *meso*-phenyl rings or introduction of bulky peripheral substituents in the *β*- and *meso*-positions of the OEP

molecule lead to distortions of π-conjugated macrocycle from planarity even in the ground S_0 state, considerably changing its geometry and electronic structure, followed by the perturbation of the energy level structure and strengthening of the non-radiative deactivation channels $S_1 \sim\sim > S_0$ and $T_1 \sim\sim > T_0$ for excited S_1 and T_1 states.

It should be mentioned in this respect that using NO_2-group as an electron acceptor did not seem to be promising enaugh because of relatively small PET rate constants with respect to those obtained for numerous synthetic porphyrin-quinone D-A pairs.[56,57] But nevertheless, we found[58-60] that namely steric hindrance interactions in *meso-ortho*-nitrophenyl substituted molecules OEP-Ph(o-NO_2) and PdOEP-Ph(o-NO_2), and in their chemical dimers (see structures A and B in Figure 1) may enhance significantly PET rate constants and efficiency. Below we discuss main results and conclusions obtained for these compounds on the basis of spectral-kinetic measurements (Table 1) and the corresponding calculations.

Figure 5. Principal schemes of laser picosecond fluorescent setup (A) and femtosecond pump-probe setup for spectral-kinetic measurements of transient states (B).

Table 1. Kinetic parameters of S_1 and T_1 states for OEP-Ph molecules at 295 K in toluene and dimethylformamide (*).

Compound	φ_F	τ_S, ns	φ_P^0	τ_T, ns	τ_T^0, ns
OEP-Ph(o-CH_3)	0.07	11.4	—	370	1000
OEP-Ph(o-NO_2)	0.002 0.0003*	0.125 0.040*	—	700	0.75
PdOEP-Ph(o-CH_3)	3.2·10⁻⁴ 2.8·10⁻⁴*	0.0136 —	0.03	200	85
PdOEP-Ph(o-NO_2)	1.4·10⁻⁴ 0.5·10⁻⁴*	0.007 ~0.003*	~10⁻⁵	0.046 0.020*	0.65 0.25*

Notes: φ_F and φ_P are quantum yields of fluorescence and phosphorescence in non-degassed solution; τ_S are fluorescence decays in non-degassed solution; values of τ_T and τ_T^0 are values obtained on the basis of ps transient absorption measurements in non-degassed and degassed solutions, correspondingly; τ_T and τ_T^0 values reflect the recombination of the radical ion pair for nitro-phenyl substituted molecules.

Table 2. Energies of locally excited S_1 and T_1 states and PET parameters for OEP-Ph(o-NO$_2$) and PdOEP-Ph(o-NO$_2$).

Compound	$E(S_1)$, eV	$E(T_1)$, eV	$E(CT)$, eV	λ_{solv}, eV	λ, eV	ΔG^0, eV		ΔG^*, eV		k^S_{PET}, s^{-1}	k^T_{PET}, s^{-1}
						$S_1 \rightarrow CT$	$T_1 \rightarrow CT$	$S_1 \rightarrow CT$	$T_1 \rightarrow CT$		
Toluene ($\varepsilon = 2.38$), 295 K											
OEP-Ph(o-NO$_2$)	1.96	1.54	1.78	0.03	0.23	-0.18	+0.24	0.003	—	8.0·10^9	—
PdOEP-Ph(o-NO$_2$)	2.23	1.84	1.79	0.03	0.23	-0.44	-0.05	0.05	0.035	7.0·10^{10}	2.2·10^{10}
Dimethylformamide ($\varepsilon = 36.7$), 295 K											
OEP-Ph(o-NO$_2$)	1.97	1.54	1.75	0.45	0.65	-0.22	+0.21	0.07	—	2.5·10^{10}	—
PdOEP-Ph(o-NO$_2$)	2.24	1.85	1.76	0.45	0.65	-0.48	-0.09	0.01	0.12	2.6·10^{11}	5.0·10^{10}

Notes: Calculations of rate constants k_{PET} for the photoinduced electron transfer from S_1 states, k^S_{PET}, and T_1 states, k^T_{PET}, were done according to well-known expression $k_{PET} = 1/\tau - 1/\tau^0$, where τ^0 and τ are decays of unquenched and quenched S_1 or T_1 states. Calculations of other parameters for PET with participation of for S_1 and T_1 states were carried out using the corresponding Equations (1-4).

It is seen from Table 1 that the fluorescence quantum yield of OEP-Ph(o-NO$_2$) is decreased by 35 times with respect to that for OEP-Ph(o-CH$_3$) in toluene at 295 K, and in polar dimethylformamide (DMF) this quenching becomes stronger. Time-resolved measurements show also that for OEP-Ph(o-NO$_2$) molecule the relaxation time of S_1 state is equal τ_S=125 ps while for OEP-Ph(o-CH$_3$) molecule τ_S=11.4 ns in toluene at 295 K. Data presented in Table 1 show that in polar DMF this shortening becomes stronger τ_S=40 ps for OEP-Ph(o-NO$_2$). In the case of Pd-complexes the tendency is the same: for PdOEP-Ph(o-CH$_3$) molecule τ_S=13.6 ps, while for PdOEP-Ph(o-NO$_2$) molecule τ_S=7.4 ps in toluene and 3 ps in DMF. S_1 state molecule decays with τ_S=13.6 ps In addition, for PdOEP-Ph(o-NO$_2$) S_1 state decay shortening is accompanied by the decrease of the fluorescence efficiency by 2.3 times with respect to that for PdOEP-Ph(o-CH$_3$). Finally, it should be noted that at 77 K in glassy matrixes, fluorescence lifetimes for PdOEP-Ph(o-CH$_3$) and PdOEP-Ph(o-NO$_2$) coincide practically. Taken together, all these results for OEP-Ph(o-NO$_2$) and PdOEP-Ph(o-NO$_2$) molecules demonstrate the existence of the effective PET OEP$\rightarrow$ NO$_2$ in *meso-ortho*-nitrophenyl substituted octaethylporphyrins taking place in a picosecond time scale.

According to the semiclassical Marcus theory,[22,25,56,57] at high temperatures the rate constant k^S_{PET} for endergonic or moderately exergonic non-adiabatic PET within the "normal" region is given by the following expressions:

$$k^S_{PET} = \frac{2\pi}{\hbar} \cdot \frac{V^2}{\left(4\pi\pi\lambda_B T\right)^{1/2}} \cdot exp\left(-\frac{\Delta G^*}{k_B T}\right) \quad (1)$$

$$\Delta G^* = \frac{\left(\Delta G^0 + \lambda\right)^2}{4\lambda} \quad (2)$$

Here k_B is Boltzman's constant, T is the temperature, h is Plank's constant, V is the electronic coupling term between the electronic wave functions of the reactant and product states, $\lambda = \lambda_{in} + \lambda_{solv}$ is the Gibbs reorganisation energy (determined by the nuclear λ_{in} and solvent λ_{solv} reorganisation energies), ΔG^0 is the standard Gibbs energy of the PET reaction, ΔG^* is the Marcus Gibbs activation

energy. For porphyrins that do not undergo substantial geometry changes upon one-electron redox events $\lambda_{in} \approx 0.2$ eV.[22,25,56] The solvent reorganization energy λ_{solv} is often calculated according to[22,25]

$$\lambda_{solv} = \frac{e^2}{4\pi\varepsilon_0}\left[\frac{1}{2r_D} + \frac{1}{2r_A} - \frac{1}{r_{DA}}\right]\left[\frac{1}{\varepsilon_{op}} - \frac{1}{\varepsilon_{ct}}\right], \quad (3)$$

where e is the charge transferred, $\varepsilon_{op} = n^2$ is the optical dielectric constant, n is the refraction index and ε_{st} is the static dielectric constant of the solvent. Based on the literature data and the HyperChem optimised OEP-Ph(o-NO$_2$) geometry, the following parameters were obtained:[58] r_D= 5 Å, r_A= 3.5 Å, r_{DA}=5.7 Å and λ_{solv}=0.5 eV, λ=0.7 eV.

In the case of ET from the singlet excited state c of the reaction is given by[22,25,56,61]

$$\Delta G^0 = e(E^{ox}_{1/2} - E^{red}_{1/2}) - W - E_{S1} \quad (4)$$

For OEP-Ph(o-NO$_2$) molecule $\Delta G^0 = -0.16$ eV, and ΔG^*=0.1 eV. Thus $\left|-\Delta G^0\right| < \lambda$, and PET process in this case may be assigned to the "normal" region of the Marcus parabolic dependence, $\log(k^S_{PET}) = f(-\Delta G^0)$.

All calculated PET parameters for OEP-Ph(o-NO$_2$) and PdOEP-Ph(o-NO$_2$) molecules in toluene and DMF are collected in Table 2 where calculated rate constants for PET from S_1 states, k^S_{PET}, and T_1 states, k^T_{PET} are presented also.

It is seen from Table 2 that for OEP-Ph(o-NO$_2$) and PdOEP-Ph(o-NO$_2$) molecules the rate constant k^S_{PET} increases significantly on going from toluene to DMF. This rise reflects the increase of the electronic coupling term V^S_{12} (calculated using Eq. 1) upon the solvent polarity rise (transition from toluene to DMF) due to the fast polarization-induced orientational rearrangements of the solvate shell in polar media: V^S_{12}=7 cm^{-1} $\rightarrow$ V^S_{12}=70 cm^{-1} for OEP-Ph(o-NO$_2$) and V^S_{12}=14 cm^{-1} $\rightarrow$ V^S_{12}=56 cm^{-1} for PdOEP-Ph(o-NO$_2$). The data of Table 2 show also that for PdOEP-Ph(o-NO$_2$), the rate constants k^T_{PET} are somewhat smaller than k^S_{PET} values. A possible reason of that may be connected with a different character of distribution of the local electron densities of the porphyrin macrocycle in S_1 and T_1 states caused by distinct overlap with molecular orbitals of NO$_2$ group in the conditions steric hindrance interactions.
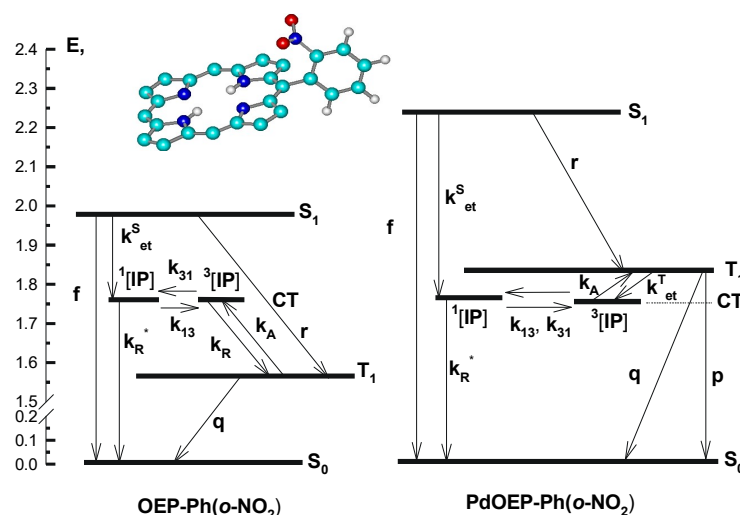
Figure 6. Schematic energy level diagram for low-lying locally excited S_1 and T_1 states, charge-transfer states CT and decay pathways for OEP-Ph(o-NO$_2$) and PdOEP-Ph(o-NO$_2$) at 295 K. Rate constants of the following processes are shown: f, fluorescence $S_1 \rightarrow S_0$; r, inter-system crossing $S_1 \sim \sim > T_1$; p, phosphorescence $T_1 \rightarrow S_0$; q, non-radiative deactivation $T_1 \sim \sim > S_0$; k^S_{PET} and k^T_{PET}, PET with participation of S_1 and T_1 states, correspondingly; k_A, thermally activated population of higher lying states; k_{31} and k_{13}, spin dephasing ion-radical pair; k_R^* and k_R, recombination of singlet and triplet ion-radical pair, correspondingly; ^{1}[IP] and ^{3}[IP], singlet and triplet states of ion-radical pair. Top: Optimized geometry of OEP-Ph(o-NO$_2$) molecule (calculations on the basis of HyperChem software package, release 4, semiempirical method PM3).

Finally, it should be mentioned that, in contrast to PET rate constants obtained at ambient temperature in non-polar solvents for nitroporphyrins with other displacement of NO$_2$ groups as well as for tetraazapophyrins with nitrogroup and nitro-phenyl substituted TPP derivatives, our results for these *meso-ortho*-nitrophenyl substituted OEP-Ph(o-NO$_2$) molecules give k^S_{PET} values by 1–2 orders of magnitude higher and demonstrate that steric hindrance effects and the nature of the linkage between D and A influence significantly on the efficiency and the mechanism of PET. In our case, for mono-*meso*-phenyl substituted OEP and their chemical ephras containing the NO$_2$ group in the *ortho*-position of the phenyl ring, steric interactions between bulky C$_2$H$_5$ substituents in β-positions of pyrrole rings and NO$_2$ group favor the efficient electronic interaction between the donor and the acceptor thus leading to efficient quenching of the porphyrin fluorescence due to the direct PET from the S_1 state to a low-lying charge-transfer state (CT) via "through-space" mechanism. Quantum-chemical calculations show[62] that the lowest unoccupied molecular orbital of the OEP-Ph(o-NO$_2$) molecule is almost completely localized at the nitro group (93.8%) and has only a small admixture (3.3%) of atomic orbitals of the porphyrin macrocycle. According to these calculations, a nonzero contribution of the atomic orbitals of NO$_2$ group to the porphyrin e_{gx} orbital (2.7%) is typical for OEP-Ph(o-NO$_2$), which indicates a direct overlap of porphyrin π-orbitals with the lowest unoccupied molecular orbital of NO$_2$ group. As we discussed above, for *ortho*-NO$_2$ containing compounds steric interactions of C$_2$H$_5$ groups at the β-pyrrolic positions flanking bulky *ortho*-NO$_2$ substituents in the phenyl ring lead to libration motions of the phenyl ring to be strongly hindered. Thus, for such certainly more conformationally rigid *D-A* pair the spin-exchange energy is negligible and the spin rephasing between the singlet and

triplet radical ion pairs is rather effective with the corresponding rate constants of $k_{13} \approx k_{31} \approx 5.0 \cdot 10^7 \, \text{s}^{-1}$ (Figure 6).

However, in the dimer OEP-Ph-OEP-Ph(o-NO$_2$) k^S_{PET} is reduced by three times relative to that for the corresponding monomer OEP-Ph(o-NO$_2$). It seems reasonable to propose that this reduction is connected with the existence of the competing non-radiative S-S energy migration between covalently linked porphyrin macrocycles (with the rate constant of $F^{SS}=(1.9–5.0) \cdot 10^9 \, \text{s}^{-1}$).

Concluding, results described in this section evidently show that the photophysical consequences of the dynamic non-planarity of *meso*-phenyl substituted octaethylporphyrins in excited states should be included in the quantitative estimation of the quenching efficiency for the corresponding porphyrins with NO$_2$ groups and more complex arrays on their base.

2. Photoinduced electron transfer in porphyrin chemical dimers covalently linked with electron acceptor

It was shown by us earlier[10,11,43] that at 293 K absorption spectra of porphyrin chemical dimers (ZnOEP)$_2$Ph-A with covalently linked Q and Pim (see Figure 3) are identical with that obtained for pure dimer. These observations provide good evidence for the absence of ground-state interactions between the dimer tetrapyrrole rings and attached Q or Pim acceptors.

Nevertheless, in contrast to the pure dimer (ZnOEP)$_2$Ph (fluorescence decay $\tau_S^0 = 1.21$ ns in toluene at 293 K), the essential fluorescence quenching is observed for (ZnOEP)$_2$Ph-A systems at the same conditions ($\tau_S = 34$ ps for (ZnOEP)$_2$Ph-Q and ($\tau_S = 135$ ps for (ZnOEP)$_2$Ph-Pim, Table 3). In addition, femtosecond transient absorption spectra show a noticeable spectral dynamics depending on delay time and the registration wavelength (Figure 7A,B).

In the case of (ZnOEP)$_2$Ph-Q the decay value derived from the time evolution of the transient absorbance at 680 nm corresponds to the dimer locally excited S$_1$ state deactivation within τ_S=25 ps in toluene at 293 K. The picosecond fluorescent TCSPC method gives τ_S=34 ps in toluene (Table 3) and τ_S=27 ps in toluene+pyridine at ambient temperature. For (ZnOEP)$_2$Ph-Pim dimers, femtosecond transient absorption data show the absorption bands rising near 670 nm and 715 nm (Figure 7B) which we ascribed to ZnP$^+$ and Pim$^-$ species, respectively, by referring to the corresponding spectra obtained by electrochemical oxidation of ZnOEP[66] and reduction of Pim.[42] Transient absorption decays measured at 670 nm and 715 nm coincide within experimental error manifesting themselves the existence of one-step PET from a locally excited S$_1$ state of the dimer (ZnOEP)$_2$Ph to the electron acceptor ^{1}Dimer*...Pim → Dimer$^+$...Pim$^-$. The comparison of data presented in Table 3 and Figure 7 indicates a reasonable agreement between results obtained via picosecond fluorescent measurements (TCSPC method) and by femtosecond pump-probe technique.

The analysis of PET events being obtained for (ZnOEP)$_2$Ph-Q and (ZnOEP)$_2$Ph-Pim dimers, having the same geometry but different acceptors shows the following. For these systems in the given conditions, the semi-classical Marcus theory of endergonic or moderately exergonic non-adiabatic PET occurring within the "normal" region,[22,25,56,57] may be applied also. Thus, the application of Equations 1–4 is correct in this case (see Notes to Table 3).

With the assumption that the standard Gibbs energy ΔG^0 and the reorganisation energy λ are temperature independent, the estimation of λ value and the electronic coupling term V may be done from the experimental dependence of k_{PET} on temperature according to:[67]

$$ln\left[k_{ET}(\lambda T^{1/2}\right] = C_2 - \frac{\Delta G^*}{k_B T}, \qquad (5)$$

$$\text{where} \quad C_2 = ln\left[\frac{4\pi^2}{h} \cdot \frac{V^2}{(4\pi 4_B)^{1/2}}\right] \qquad (6)$$

Using this approach, our TCSPC data for (ZnOEP)$_2$Ph-Pim in toluene and toluene+pyridine in a temperature range of 273–196 K were fitted (see Figure 7C). The presented results show that the data for both solvents fall on linear plots with good correlation coefficients. Estimated nuclear and electronic factors are as follows: λ = 0.243 eV, V = 1.18 meV (toluene) and λ = 0.417 eV, V = 2.12 meV (toluene+pyridine). Taking into account that nuclear factors λ do not differ significantly for two dimers of the same geometry, (ZnOEP)$_2$Ph-Q and (ZnOEP)$_2$Ph-Pim, and different values of ΔG^0 (Table 3) one obtains the corresponding values of the electronic coupling for quinone-substituted dimer: V = 2.35 meV (toluene) and V = 4.22 meV (toluene+pyridine).

Table 3. Structural and photophysical parameters for the dimer (ZnOEP)$_2$Ph-A with covalently linked acceptors at T=295 K.

Dimer-A	$E(S_1^D)$, eV	E_A^{red}, eV	r_A, Å	r_{DA}, Å	$E(IP)$, eV	ΔG^0, eV	τ_S, ps	$k_{ET}\cdot 10^{10}$, s^{-1}
(ZnOEP)$_2$Ph-Q	2.13	-0.45	3.3	10.8	1.72	-0.41	34	2.86
(ZnOEP)$_2$Ph-Pim	2.13	-0.76	3.5	13.0	2.00	-0.13	135	0.66

Notes: The energy level of the dimer locally excited S$_1$ state $E(S_1^D)$ was determined on the basis of the fluorescence and absorption Q(0,0) bands. One electron reduction potentials E_A^{red} (in dimethylformamide) were taken for Pim E_A^{red} = –0.76 V,[42] and for Q $E_{1/2}^{red}$ = –0.45 V.[63] One electron oxidation potential for the dimer (ZnOEP)$_2$Ph was used as $E_{1/2}^{ox}$=0.74 V.[64] Acceptor r_A radii for Q[25] and Pim[40,42] were taken from literature. Radius of the donor (ZnOEP)$_2$Ph and intercenter distances r_{DA} were estimated on the basis of molecular modeling (HyperChem software package, release 4, semiempirical method PM3). The energy levels of the ion pair states in toluene were estimated according to [65]: $E(IP) = e(E_D^{ox} - E_A^{red}) + \Delta G_S$, where the standard Gibbs energy ΔG^0 and Marcus Gibbs activation energy ΔG^* were calculated using Equations 2–4 presented in previous section. PET rate constants k_{ET} were calculated using the formulae $k_{ET} = 1/\tau_S - 1/\tau_S^0$, where τ_S^0=1.21 ns is fluorescence decay of pure dimer (ZnOEP)$_2$Ph in toluene, τ_S is S$_1$ state decay measured for (ZnOEP)$_2$Ph-A systems.

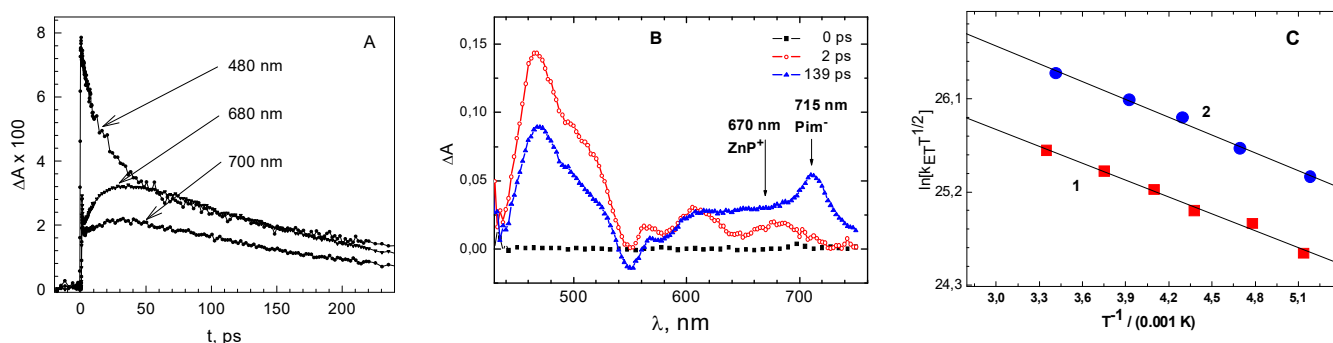**Figure 7.** Time profiles in transient absorption spectra of ZnOEP)$_2$Ph-Q measured at 480 nm, 680 nm and 700 nm (**A**, λ_{pump}=400 nm), and time-resolved absorption spectra of (ZnOEP)$_2$Ph-Pim at delay times 0 ps, 2 ps and 139 ps (**B**, λ_{pump}=540 nm) in toluene at 293 K. (**C**) Analysis of the temperature dependence of k_{PET} for ZnOEP)$_2$Ph-Pim in toluene (1) and toluene+pyridine (2) using Eq.(6). Experimental dependencies are fitted by a linear function y =mx + y$_0$, where $y_0 = ln\left(\frac{2\pi V^2}{h}\sqrt{\frac{\pi}{\lambda k_B}}\right)$ and $m = -\frac{(\Delta G^0 + \lambda)^2}{4\lambda k_B}$

It is known,[66] that PET reactions are non-adiabatic by Landau-Zener criteria if they satisfy the following relationship

$$4\pi^2 V^2/h\,\omega(2\lambda k_B T)^{1/2} < 1\ ,\qquad(7)$$

where $\omega \sim 100$ cm^{-1} for typical low-frequency solvent motions at 300 K. It follows from above presented data that for (ZnOEP)$_2$Ph-Q$_1$ and (ZnOEP)$_2$Ph-Pim dimers this criterion is operative. Thus, assuming realistic errors for λ and ΔG^0 estimations one may conclude that at 293 K the dimer S$_1$ state quenching is due to the non-adiabatic PET.

Finally, one principal moment should be mentioned: for the dimer (ZnOEP)$_2$Ph-Q the PET rate constant in toluene at 293 K ($k_{PET}=2.86\cdot10^{10}$ s^{-1}, Table 3) is smaller, essentially if compared to those found for monomeric ZnP-Q compounds with the same r_{DA} distances, and near ΔG^0 values ($k_{PET}= (1.6–6.0)\cdot10^{11}$ s^{-1} in benzene at 293 K[68]). The reason of that is explained definitely if one takes into account the competition between the non-radiative S-S energy migration among dimer subunits and charge separation. According to experimental findings and theoretical estimations,[11,11,27] for Zn-porphyrin chemical dimers with intercenter distances of $r_{DA} \approx 11–13$ Å, rate constants of the non-radiative S-S energy migration are of $k_{EM} \approx (3–7)\cdot10^{10}$ s^{-1}. Correspondingly, as far as for the dimer (ZnOEP)$_2$Ph-Q $k_{EM} \leq k_{PET}$, a slower energy transfer process limits the fast PET leading to the relative decrease of the experimental k_{PET} values with respect to those found for quinone substituted monomers. In contrast, for the dimer (ZnOEP)$_2$Ph-Pim the inverse situation realises: $k_{EM} \geq k_{ET}$. Correspondingly, in the latter case the experimental k_{ET} values are of the same order of magnitude for dimers and monomers.

3. Photoinduced electron transfer in self-assembled porphyrin triads: role of the solvent polarity and temperature

One major purpose of our approach in this direction was to mimic some aspects and functionalities of chlorophylls within photosynthetic systems *in vivo*. As outlined in Introduction, the main challenge in making porphyrin-based systems that mimic the primary photoevents taking place in natural objects lies in the preparation of multiporphyrin complexes of predicted composition and morphology where subunits may be coupled via both covalent and non-covalent bonds. Such an approach has been realized by us upon formation and study of various multicomponent arrays containing tetrapyrrole macrocycles.[4,10,11,27,28.39,43,69-73] In this section, we quantitatively discuss some peculiarities of PET processes which have been found and studied in self-assembled porphyrin triads of the same structure formed via coordinative interactions of two Zn ions of the porphyrin chemical (ZnOEP)$_2$Ph with dipyridyl-substituted porphyrin free bases (as extra-ligands) such as H$_2$P and its pentafluorinated derivative (H$_2$PF) (optimized geometries of the triads **I** and **II** are presented in Figure 5).

Our previous results reveal[4,10,11,73] that in non-polar solvents at ambient temperature, the formation of 1:1 self-assembled triads is realized during a titration of the dimer

(ZnOEP)$_2$Ph solution by solutions of various dipyridyl-containing porphyrin free bases (extra-ligands). In all cases absorption spectra of the triads are essentially a linear combination of the corresponding dipyridinated dimer (ZnOEP)$_2$Ph and extra-ligand, with only small differences in wavelength maxima and band shapes. It means that the interaction between the two subunits is weak in the ground state, and they retain their individual identities.

It is seen from Figure 8B that for the triad (ZnOEP)$_2$Ph$\otimes$H$_2$P(m^Pyr)$_2$-(iso-PrPh)$_2$ fluorescence spectra do show strong quenching of the dimer (ZnOEP)$_2$Ph fluorescence (short wavelength bands), and the final emission of the triad mainly consists of the extra-ligand fluorescence bands (long wavelength ones). In toluene at 293 K, excitation fluorescence spectra of the triad ($\lambda_{det} > 720$ nm, the ligand emission) clearly show the existence of absorption bands of the dimer (549 nm and 587 nm). Correspondingly, it seems reasonable to explain these facts by the singlet-singlet energy migration (EM) Zn-dimer*$\rightarrow$extra-ligand. The detailed analysis of EM events for these triads shows[74,75] that EM rate constants $[k_{EM}= (1/\tau_S)(R_0^{theor}/ r_{DA})^6]$ are in the range of $k_{EM}= (6.7–7.5)\cdot10^{10}$ s^{-1}. It means that the lifetime of the dimer S$_1$ state should be in the range of 15–13 ps.

Nevertheless, the real dynamics of the electronic energy deactivation in the given triad is not governed by only one EM process. It follows from TCSPC measurements (Figure 9A, Table 4) that in the triad, the fluorescence of the extra-ligand H$_2$P(m^Pyr)$_2$-(iso-PrPh)$_2$ is reduced noticeably with respect to that for uncomplexed porphyrin. Moreover, upon the solvent polarity rise (addition of acetone to toluene solution) the decay time shortening for the extra-ligand fluorescence becomes stronger accompanied by a more pronounced decrease of its fluorescence quantum yield. Figure 8C shows also that the increase of the solvent polarity manifests itself into two transformations of fluorescence excitation spectra of the triads: *i)* the decrease of the extra-ligand whole fluores-cence intensity, and *ii)* at 17 vol% of acetone admixture in toluene the form of the excitation spectrum of the triad changes becomes almost identical to that of the individual extra-ligand H$_2$P(m^Pyr)$_2$-(iso-PrPh)$_2$. This indicates that the sensitisation effect due to EM Zn-dimer*$\rightarrow$extra-ligand is absent in the last case, though the usual through-space singlet-singlet energy transfer in multiporphyrins arrays is hardly dependent on solvent polarity.[4,10,11,20,21] At the same time, the dimer emission in the triad remains strongly quenched upon the solvent polarity increase. These observations for the extra-ligand in the triad can therefore not be explained by EM processes to lower lying locally excited states. Rather the possibilities of PET have to be considered.

Experimental femtosecond pump-probe results for the triad (ZnOEP)$_2$Ph$\otimes$H$_2$P(m^Pyr)$_2$-(iso-PrPh)$_2$ evidently show (Figure 8B,C) the bleaching of the porphyrin extra-ligand Q-bands at 515, 550 and 580 nm and the formation of absorption band at 680 nm usually ascribed to the Zn-porphyrin cation.[25,30,40,42] So, the formation of charge transfer (CT) states is clearly detected. From the time evolution of transients it is seen that the increase of the extra-ligand H$_2$P(m^Pyr)$_2$-(iso-PrPh)$_2$ ground state bleaching at 510 nm is observed after an immediate rise at time zero. The decay was fitted with the time constant

1.7±0.1 ps. These experimental findings may be considered as a real proof PET realization in the given triad being the main relaxation process in polar media.

For the triad $(ZnOEP)_2Ph \otimes H_2P(m^Pyr)_2$-(iso-PrPh)$_2$, the emission intensity of the extra-ligand is decreasing upon the temperature lowering. In a temperature range of 160–278 K this dependence was fitted to a Boltzman distribution function ($const + 1/(1+exp\{\Delta E/kT\})$), thus giving the activation energy for PET as $\Delta E = 0.05$ eV.

It follows from the data collected in Table 4 and calculations based on Equations 1–4, that the standard Gibbs energy $\Delta G^0 < 0$. Thus, according to Marcus theory,[22] PET in the triad $(ZnOEP)_2Ph \otimes H_2P(m^Pyr)_2$-(iso-PrPh)$_2$ is adiabatic and is realized in a "normal" region.
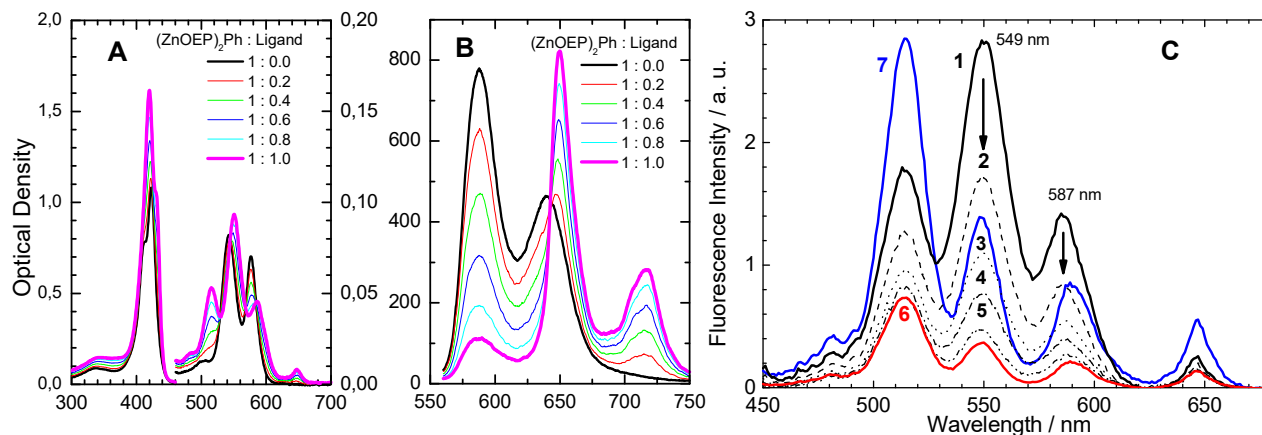
Figure 7. Absorption (**A**), fluorescence (**B**, λ_{ex}=546 nm) spectra of the dimer $(ZnOEP)_2Ph$ with increasing amounts of extra-ligand $H_2P(m^Pyr)_2$-(iso-PrPh)$_2$, as well corrected fluorescence excitation spectra of the triad $(ZnOEP)_2Ph \otimes H_2P(m^Pyr)_2$-(iso-PrPh)$_2$ (**C**, λ_{em}=720 nm). **A, B:** Bold pink curves correspond to the triad spectra (structure A in Figure 4). **C:** Curves 2, 3, 4, 5, 6 correspond to the sequential addition of 0, 3, 6, 9, 17 vol% of acetone (thin dashed lines, intensity decreases with increasing amount of acetone). Curve 7 presents the excitation spectrum of $H_2P(m^Pyr)_2$ alone in toluene at the same concentration as in the triad.
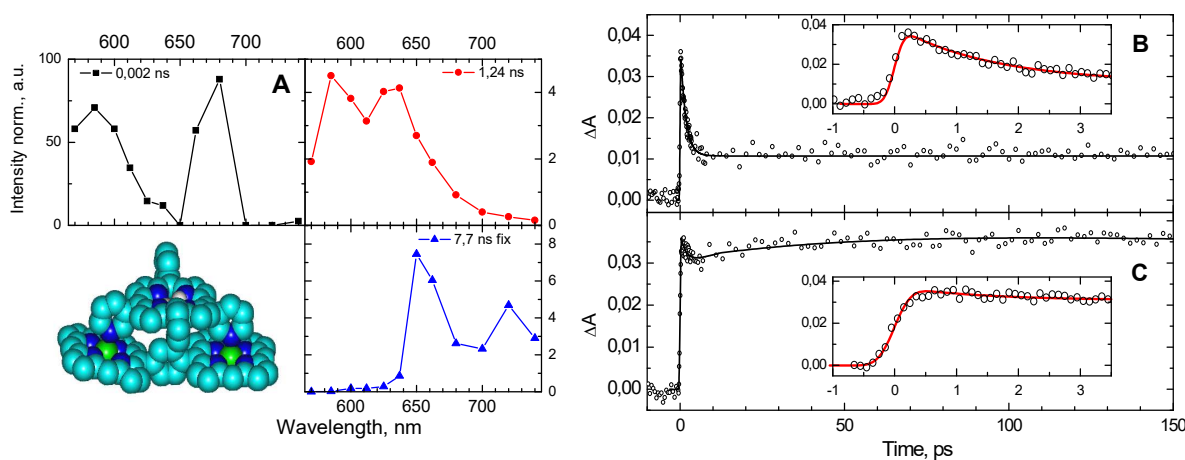
Figure 9. Decay-associated spectra (λ_{ex} = 546 nm) derived from global analysis of 12 TCSPC time-resolved fluorescence measurements (**A**) and time evolution of transient absorbance of the triad $(ZnOEP)_2Ph \otimes H_2P(m^Pyr)_2$-(iso-PrPh)$_2$ pumped at 555 nm and probed at 515 nm (**B**) and 680 nm (**C**) in toluene at 295 K. Optimized geometry of the triad was calculated using HyperChem software package, release 4, semiempirical method PM3.

Table 4. Structural and PET parameters for triad based on the dimer $(ZnOEP)_2Ph$ and porphyrin extra-ligands (toluene, 295 K).

Triad type	r_{DA}, Å	E_A^{red}, eV	$E(S_1^L)$, eV	τ_{S0}^{Dim}, ns	τ_{S0}^L, ns	τ_S^L, ns	ΔG^0, eV	$E(IP)$, eV
$(ZnOEP)_2Ph \otimes_2Ph \otimes H_2P(m^Pyr)_2$	8.8	-0.98	1.91	1.15	9.5	7.7	0.287	1.90
$(ZnOEP)_2Ph \otimes H_2P(m^Pyr)_2$-(5FPh)$_2$	8.8	-0.98	1.91	1.15	9.4	0.02	0.287	1.75

Notes: Intercenter distances r_{DA} were estimated from optimised structures of the triads (Figure 4). The oxidation potential for coordinated dimer $(ZnOEP)_2Ph$ was taken to be E_D^{ox}=0.63 V. τ_{S0}^{Dim} is the measured fluorescence decay for an individual dimer in toluene+pyridine. τ_{S0}^L and τ_S^L values are the fluorescence lifetimes for the individual extra-ligand and in the triad, correspondingly (based on TCSPC measurements). The energy levels of the extra-ligand locally excited S$_1$ states $E(S_1^L)$ were determined on the basis of the corresponding fluorescence and absorption Q(0,0) bands. The energetic parameters ΔG_S and $E(IP)$ were estimated according to approach described in above presented Tables.

On the other hand, for the triad (ZnOEP)$_2$Ph⊗H$_2$P(m^Pyr)$_2$-(5FPh)$_2$ containing penta-fluorinated extra-ligand (known as a strong electron acceptor[64]), the obtained spectral and time-resolved results show completely different behavior. The fluorescence excitation spectrum in this case is identical to that of the pure H$_2$P(m^Pyr)$_2$-(5FPh)$_2$ indicating that no fluorescence is sensitized via (ZnOEP)$_2$Ph. From ambient temperature down to 164 K no sensitized fluorescence of the extra-ligand is observed. Time-resolved spectra of this triad (presented in Figure 10) show the ground state bleaching of the porphyrin Q-bands at 515, 550 and 580 nm (assigned to the free base absorption) and a broad absorption at around 680 nm (usually ascribed to the Zn-porphyrin cation[68]). The corresponding decay times were fitted with time constant 0.7±0.1 ps. In addition, almost no change of the bleaching signal of the dimer (at 550 and 580 nm) was found which clearly indicates that the excited dimer does not return to its ground state during this time. Therefore, it does not transfer its energy to the extra-ligand H$_2$P(m^Pyr)$_2$-(5FPh)$_2$ and the increased bleaching at 510 nm is attributed to production of the extra-ligand radical anion. Summarizing we argue that in this triad, an extremely fast PET process takes place on a time scale of 0.7 ps. Moreover, as there is no increase of free-base fluorescence in the steady-state spectra upon lowering of temperature down to 164 K one may conclude that this PET is still effective at 164 K. Such low temperature PET is rare phenomenon.

This PET process has to be compared to the one observed in a similar system,[76] where a Zn-porphyrin is covalently linked to a free base porphyrin with three penta-fluorophenyl substituents, and PET is realized within 71 ps, while the decay of the charge separated state is even faster (8 ps^{-1}). In our case, PET takes place within a much shorter time. We attribute this to much increased overlap of donor and acceptor electronic wave functions as in this case the dimer (ZnOEP)$_2$Ph and fluorinated extra-ligand H$_2$P(m^Pyr)$_2$-(5FPh)$_2$ are face to face with a short distance between the porphyrin planes of approximately 3.5 Å, while in the covalently linked system.[76] D and A are edge-to-edge at large distance of approximately 14 Å. The measured transient times in our case for artificial system resembles more those observed in bacterial photosynthesis of a few 100 fs to a few ps.[77] These natural systems too do show efficient charge transfer at low temperatures[78] while only few model systems with this property have been described.[79] We ascribe the high efficiency of PET at low temperature to stabilization of the ZnP$^+$ radical cation by the pyridyl ligands.

Finally, one may conclude that the deactivation of the extra-ligand S$_1$ state in the triads **I** and **II** is complex, depends on on redox properties of extra-ligands also and governed by the competition of EM and PET processes governed by polarity and temperature of surrounding in some cases (see schematic energy level diagram in Figure 11).

Thus, the complex S$_1$ state dynamics results in a noticeable τ_S shortening and fluorescence quantum yield φ_F decrease observed for extra-ligands in the triads I and II with respect to those for individual porphyrin free bases. In fact, the presented scheme explains the existence of stimulated fluorescence of the extra-ligand in pure toluene at 293 K as a result of simultaneous realisation of EM dimer*→Ligand, PET and repopulation processes. In the triad I, the increase of the solvent polarity (addition of acetone) leading to a charge transfer (CT) state lowering manifests itself in the extra-ligand fluorescence additional quenching and the absence of sensitising effect. Because of fast competing charge transfer processes in both triads, the direct intersystem crossing S$_1$⤳⤳T$_1$ in the extra-ligand subunit is probably low effective. The population of the extra-ligand locally excited T$_1$ state may take place from the upper lying triplet radical ion pair state ^{3}(Dimer$^+$... Lig$^-$) formed via the spin rephrasing (rate constant k$_{34}$, Figure 11) between the singlet and triplet radical ion pairs.

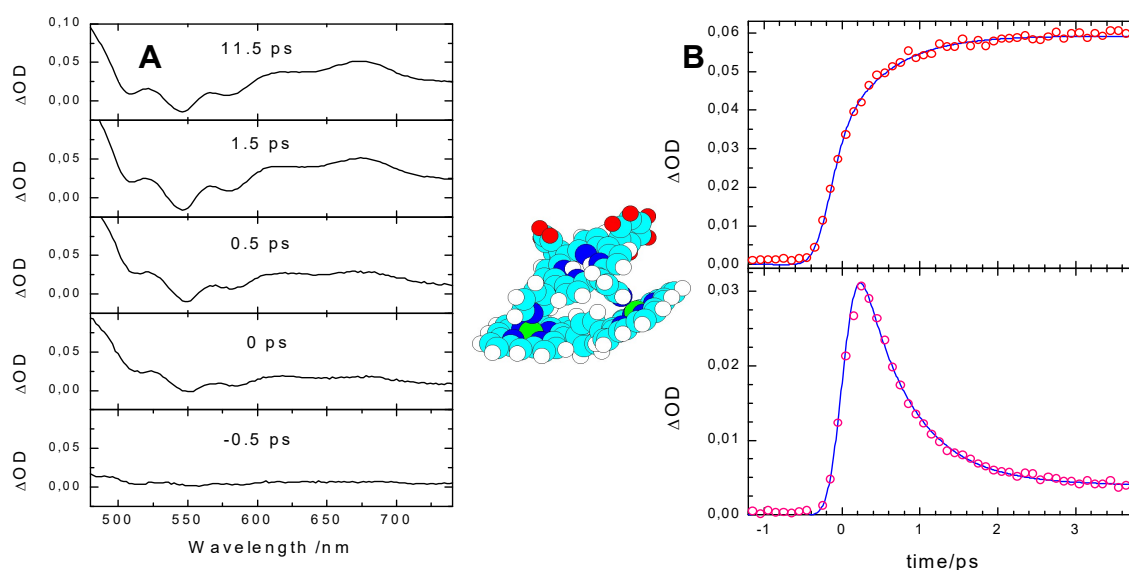**Figure 10.** Time-resolved transient absorption spectra (**A**, λ_{pump} = 400 nm) and time evolution of the transient absorbance (**B**, λ_{pump} = 555 nm) for the (ZnOEP)$_2$Ph⊗H$_2$P(m^Pyr)$_2$-(5FPh)$_2$ with fluorinated extra-ligand (structure II in Figure 4) in toluene at 293 K at various delay times and the detection wavelength. Structure of the triad was optimized on the basis of HyperChem software package, release 4, semiempirical method PM3).
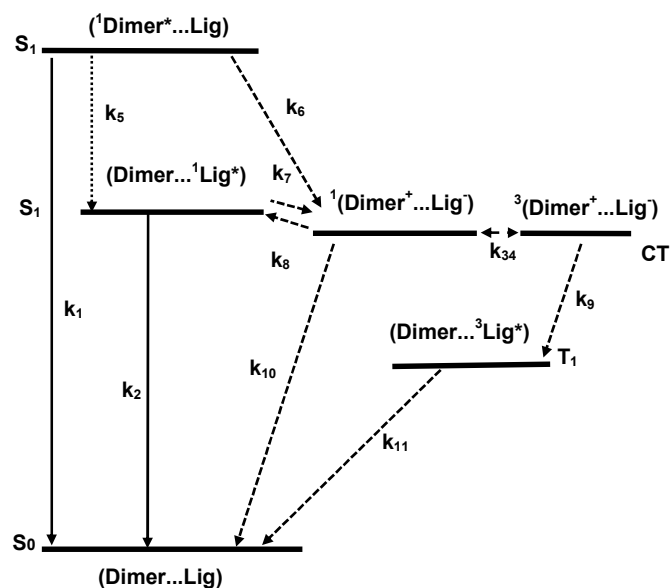
Figure 11. Schematic energy level diagram for low-lying locally excited singlet states of the dimer (ZnOEP)$_2$Ph {S$_1$,(Dimer*...H$_2$P)}, the porphyrin extra-ligand {S$_1$,(Dimer...^{1}Lig*)}, locally excited triplet state of H$_2$P {T$_1$ (Dimer...^{3}Lig*)}, radical ion pair singlet {CT, ^{1}(Dimer$^+$...Lig$^-$)} and triplet {CT, ^{3}(Dimer$^+$...Lig$^-$)} states. Indicated are rate constants of the following pathways: k$_1$, fluorescence and non-radiative decay of the dimer (ZnOEP)$_2$Ph; k$_2$, fluorescence and non-radiative decay of the extra-ligand Lig; k$_5$, S-S energy migration (ZnOEP)$_2$Ph→Lig; k$_6$, PET (ZnOEP)$_2$Ph →Lig leading to the singlet radical ion pair state formation; k$_7$, photoinduced hole transfer Lig → (ZnOEP)$_2$Ph leading to the singlet radical ion pair state formation; k$_8$, thermally activated charge recombination from the singlet radical ion pair state to the extra-ligand locally excited singlet state; k$_{34}$, spin rephasing between the singlet and triplet radical ion pairs; k$_9$, charge recombination from the triplet state of the radical ion pair to the locally excited triplet state of the extra-ligand; k$_{10}$, charge recombination from the singlet state of the radical ion pair to the ground state; k$_{11}$, non-radiative intersystem crossing T$_1$∼∼>S$_0$ from the extra-ligand locally excited state to the ground state.
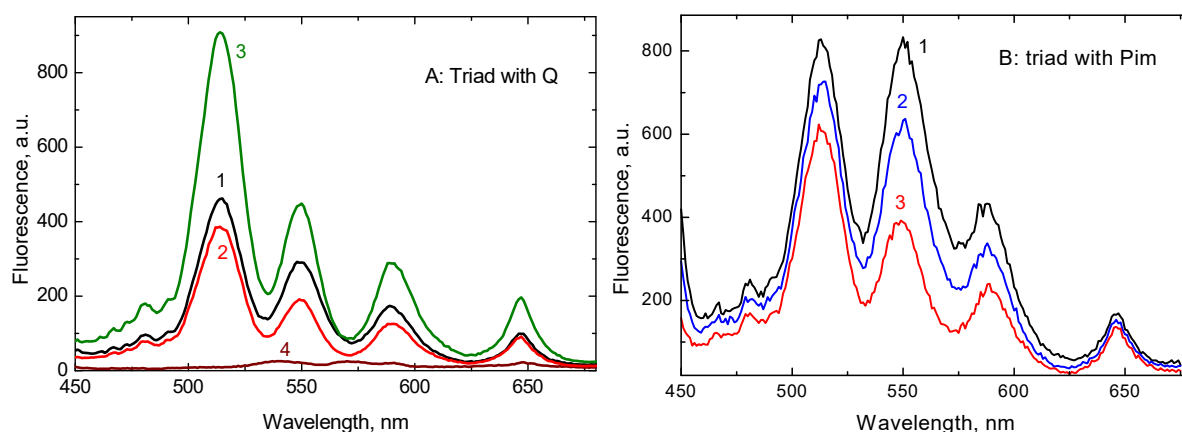
Figure 12. Fluorescence excitation spectra (λ_{em}=720 nm) of the triads (ZnOEP)$_2$Ph-Q⊗H$_2$P(m^Pyr)$_2$-(iso-PrPh)$_2$ (A), and (ZnOEP)$_2$Ph-Pim⊗H$_2$P(m^Pyr)$_2$-(iso-PrPh)$_2$ (B) upon increase of the solvent polarity at 295 K. A: pure toluene (1), + 3 vol% (2), and + 9 vol% of acetone. B: pure toluene (1) and + 9 vol% of acetonitrile (2); fluorescence excitation spectra of individual extra-ligand (3) and the dimer (ZnOEP)$_2$Ph-Q (4, multiplited by 10) in toluene.

4. Long-distant superexchange photoinduced electron transfer in self-assembled porphyrin triads with covalently linked electron acceptors

On the basis of above presented results and for the discussion here, we selected two distance-fixed systems, (ZnOEP)$_2$Ph-Q and ZnOEP)$_2$Ph-Pim with effective PET clear dynamics that were taken as the corresponding molecular blocks upon the triads formation with participation of the non-fluorinated extra-ligand: (ZnOEP)$_2$Ph-Q⊗ H$_2$P(m^Pyr)$_2$-(iso-PrPh)$_2$ and (ZnOEP)$_2$Ph-Pim⊗ H$_2$P(m^Pyr)$_2$-(iso-PrPh)$_2$ (Figure 4, structures III and IV). Like in previous cases,[4,10,11,43,75] the interaction between triad subunits is weak in the ground state, and absorption spectra of the components retain their individual properties. Our previous results[72] show that for the triads III and IV, fluorescence spectra mainly consist of the free-base extra-ligand fluorescence bands. This important observation

implies that the initial fluorescence of these triads being strongly quenched due to PET process from the dimer to Q or Pim (see Section 2), does show a remarkable additional quenching upon the triad III and IV formation in toluene at 293 K. The second found feature of the triads III and IV is that the fluorescence quantum efficiency (φ_F) of the attached extra-ligand H$_2$P(m^Pyr)$_2$-(iso-PrPh)$_2$ is smaller with respect to that for the same extra-ligand in the corresponding triads without acceptors (see Section 3) in toluene at 293 K. The decrease of φ_F values is more pronounced for Q-containing triad III with respect to that for Pim-containing triad IV.

For the triad III (ZnOEP)$_2$Ph-Q⊗H$_2$P(m^Pyr)$_2$-(iso-PrPh)$_2$ in toluene at 295 K, the fluorescence excitation spectrum is almost identical to that for the individual extra-ligand H$_2$P(m^Pyr)$_2$-(iso-PrPh)$_2$ and does not change in shape practically upon the solvent polarity rise (Figure 12A). Moreover, upon the solvent polarity rise the addi-

tional quenching of the extra-ligand fluorescence is observed, while the dimer emission in this triad remains strongly quenched. The observed experimental features for Q-containing triad may be considered as evidence that the EM process Zn-dimer*→extra-ligand is low probable compared to other non-radiative pathways. In fact, the same tendencies are observed for the triad (ZnOEP)$_2$Ph-Pim⊗H$_2$P(m^Pyr)$_2$-(iso-PrPh)$_2$ but the influence of the solvent polarity is more pronounced in the latter case (Figure 12B) as far as Pim is less efficient electron acceptor compared to Q.

TCSPC time-resolved fluorescence measurements for triads III and IV support a strong shortening of the extra-ligand excited S$_1$ state (Figure 13, Table 5). Figure 13A shows that in the Q-containing triad III, the S$_1$ state deactivation of the ligand H$_2$P(m^Pyr)$_2$-(iso-PrPh)$_2$ takes place with τ_S^L=0.94 ns, while for the same triad without quinine τ_{S0}^L=6.2 ns (Table 5) being shorter than τ_{S0} = 9.5 ns measured for individual H$_2$P(m^Pyr)$_2$-(iso-PrPh)$_2$ molecules (Table 4). As was mentioned in Section 3, the observed shortening of fluorescence decays detected for the extra-ligand in the acceptor-free triad (structure I, Figure 4)

was attributed to a photoinduced hole transfer from the extra-ligand to the dimer (rate constant k_6, Figure 11). In addition, femtosecond pump-probe data also show that the non-radiative relaxation processes for both the dimer and extra-ligand S$_1$ states are faster in Q- and Pim-containing triads with respect to those found for acceptor-free triads. In fact, presented TCSPC data reflect the final steps of the electronic energy excitation dynamics in triads III and IV.

The experimental kinetic data and comparative parameters of the energy relaxation processes in triads III and IV are collected in Table 5.

We now like to discuss possible non-radiative relaxation pathways which might cause the observed shortening of the dimer and the extra-ligand locally excited S$_1$ states in triads (ZnOEP)$_2$Ph-Q⊗H$_2$P(m^Pyr)$_2$-(iso-PrPh)$_2$ and (ZnOEP)$_2$Ph-Pim⊗H$_2$P(m^Pyr)$_2$-(iso-PrPh)$_2$ in toluene at 295 K, using schematic energy level diagram presented in Figure 14 as well as comparative results obtained for the corresponding triads without electron acceptors (Table 4, Figure 11) as well for the dimers (ZnOEP)$_2$Ph-A with covalently linked Q and Pim (Table 3).
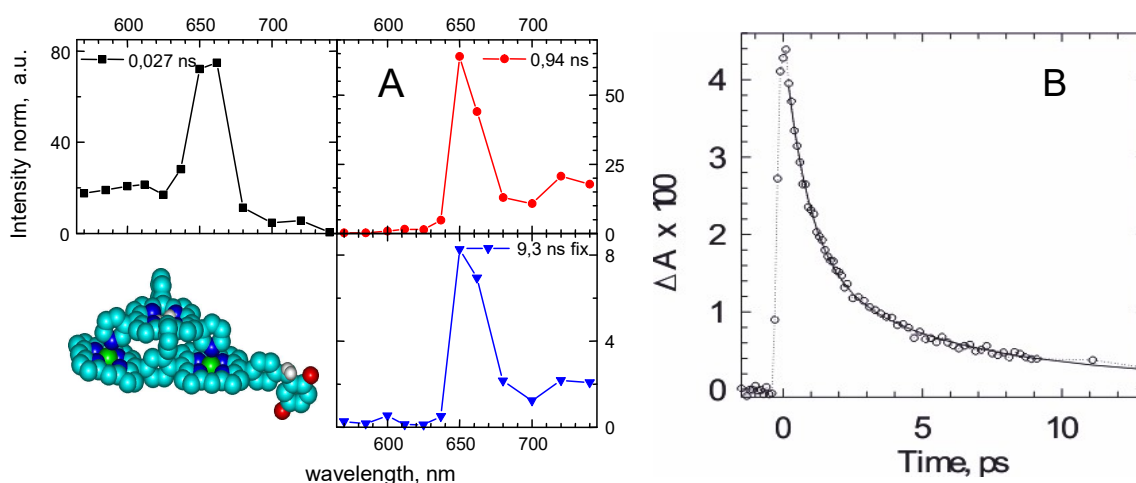

Figure 13. Decay-associated spectra of the triad (ZnOEP)$_2$Ph-Q⊗H$_2$P(m^Pyr)$_2$-(iso-PrPh)$_2$ (A) and time evolution of the transient absorbance for the triad (ZnOEP)$_2$Ph-Pim⊗H$_2$P(m^Pyr)$_2$-(iso-PrPh)$_2$ (B) in toluene at 295 K. A: λ_{ex} = 546 nm, global analysis of 12 TCSPC time-resolved fluorescence measurements. B: λ_{pump}=555 nm, λ_{det}=515 nm. Two-exponential fit I(t) = ·exp(-t) + A$_2$·exp(-t/τ_2) +δ(t) gives τ_1=0.9 ps (A$_1$= 0.029) and τ_2=5.4 ps (A$_2$= 0.015). Structure of the triad was optimized on the basis of HyperChem software package, release 4, semiempirical method PM3.
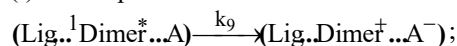
Table 5. Measured and estimated parameters for superexchange PET in triads with electron acceptors (toluene, 293 K).

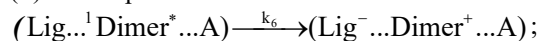| Triad	$E(S_1^D)$, eV	r_{DB}, Å	r_{DA}, Å	E_D^{ox}, eV	$E_{D^+B^-A}$, eV	τ_{S0}^D, ns	τ_S^D, ns	$k_{PET} \cdot 10^{-8}$, s^{-1}
(ZnOEP)$_2$Ph-Q⊗H$_2$P(m^Pyr)$_2$-(iso-PrPh)$_2$	1.91	8.2	18.0	1.10	3.08	6.2	0.94	9.0
(ZnOEP)$_2$Ph-Pim⊗H$_2$P(m^Pyr)$_2$-(iso-PrPh)$_2$	1.91	9.1	24.2	1.10	3.08	7.7	2.67	2.5

Notes: The energies of the extra-ligand locally excited S$_1$ state $E(S_1^D)$ was determined using fluorescence and absorption spectra. Intercenter distances r_{DB} (donor-bridge) and r_{DA} (donor-acceptor) were estimated from optimised structures of the triads. r_D = r_B 5.5 Å, acceptor radii were taken to be r_A =3.5 Å (Pim)[40,42] and r_A =3.3 Å (Q)[25]. Oxidation potentials for extra-ligands E_D^{ox} have been extracted from literature data.[80,81] The reduction potential for the coordinated dimer (ZnOEP)$_2$Ph E_B^{red} = −1.69 V.[64] The energy of mediating bridge level in toluene was estimated by $E_{D^+B^-A} = e(E_D^{ox} - E_A^{red}) + \Delta G_S$ (see Notes to Table 3). τ_{S0}^D values correspond to the extra-ligand fluorescence decay measured in triad I without electron acceptors. τ_S^D values were attributed to the complexed extra-ligand according to decay-associated spectra from TCSPC data. Rate constants k_{PET} for bridge-mediated PET were calculated by $k_{PET} = (\tau_S^D)^{-1} - (\tau_{S0}^D)^{-1}$.

It follows from the obtained results that the dimer locally excited S_1 state (Lig...^{1}Dimer...A) may be deactivated as a result of three competing non-radiative processes:

(*i*) one-step PET

$$(\text{Lig..}^1\text{Dimer}^*\text{...A}) \xrightarrow{k_9} (\text{Lig..Dimer}^+\text{...A}^-);$$

(*ii*) one-step PET

$$(\text{Lig...}^1\text{Dimer}^*\text{...A}) \xrightarrow{k_6} (\text{Lig}^-\text{...Dimer}^+\text{...A});$$

(*iii*) singlet-singlet energy migration

$$(\text{Lig...}^1\text{Dimer}^*\text{...A}) \xrightarrow{k_5} (^1\text{Lig}^*\text{...Dimer...A}).$$
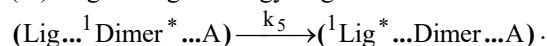
According to data discussed in Section 3 for the triads I and II, the direct one-step PET (Lig...^{1}Dimer*...A) → (Lig... Dimer$^+$...A$^-$) is low probable compared to faster processes (*ii*) and (*iii*) in triads III and IV having covalently linked Q or Pim. Nevertheless, the cooperative action of all three processes leads to the strong quenching of the dimer τ_S values in triads III and IV. Upon the solvent polarity increase, leading to CT state (Lig$^-$... Dimer$^+$...A) lowering[22,25] the process (*ii*) becomes to be dominant.

Notably, as we specifically mentioned above, in the triads containing Q and Pim, the shortening of S_1 states for the extra-ligand $H_2P(m^\wedge Pyr)_2$-(iso-PrPh)$_2$ is stronger essentially compared to that found for acceptor-free triad (*e.g.* τ_S^L = 7.7 ns in triad I, while τ_S^L =0.94 ns in triad III). Clearly, one may consider that, once formed, the locally excited S_1 state of the extra-ligand in triads III and IV may decay via two non-radiative processes:

(*i*) photoinduced hole transfer

$$(^1\text{Lig}^*\text{...Dimer...A}) \xrightarrow{k_7} (\text{Lig}^-\text{...Dimer}^+\text{...A});$$
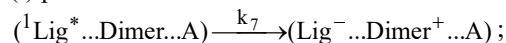
(*ii*) bridge-mediated long-distance superexchange PET[57,82-86]

$$(^1\text{Lig}^*\text{...Dimer...A}) \xrightarrow{k_{\text{superexchange}}} (\text{Lig}^+\text{...Dimer...A}^-),$$
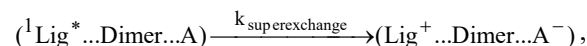
where bridge is the dimer (ZnOEP)$_2$Ph.

As has been outlined in detail,[84-86] the relatively rare realized superexchange PET occurs due to coherent mixing of three or more states of the system. Like it has been discussed for Q-containing porphyrin triads,[83] in our case these states are as follows (Figure 14): $|D^*BA\rangle$ corresponds to (^{1}Lig*...Dimer...A) state, $|D^+B^-A\rangle$ presents (Lig$^+$...Dimer$^-$...A) state, and $|D^+BA^-\rangle$ corresponds to (Lig$^+$...Dimer...A$^-$) state. Distant electron donor and acceptor can exchange their charges through the bridge, that is a high-lying "spectator" state $|D^+B^-A\rangle$ mediates the electron transfer from a donor state $|D^*BA\rangle$ to CT state $|D^+BA^-\rangle$. Within the superexchange model the charge separation rate k_{super} is proportional to ($V_{12} \cdot V_{23}$ / δE), where V_{12} and V_{23} correspond to the electronic coupling terms for PET processes $|D^*BA\rangle \rightarrow |D^+B^-A\rangle$ and $|D^+B^-A\rangle \rightarrow |D^+BA^-\rangle$, respectively, and δE is the energy difference of mediating bridge level $|D^+B^-A\rangle$ (presented in Table 5) and the crossing point of the potential energy curves of $|D^*BA\rangle$ and $|D^+BA^-\rangle$ along the reaction co-ordinate. The values of the couplings V_{12} and V_{23} are essentially lower than the energy differences between the relevant system states.

Finally, the decrease of the extra-ligand fluorescence quantum efficiency upon the solvent polarity increase, found for triads III and IV, reflects the PET rate increase in this case. According to [86] an increase in the solvent dielectric constant lowers the energies of the bridge $|D^+B^-A\rangle$ and acceptor $|D^+BA^-\rangle$ states and increases the system-bath interaction and, consequently, the relaxation coefficients. The independence of superexchange PET rates on temperature in this case could be explained[84,86] by a small temperature dependence of the Franck-Condon factor for PET.
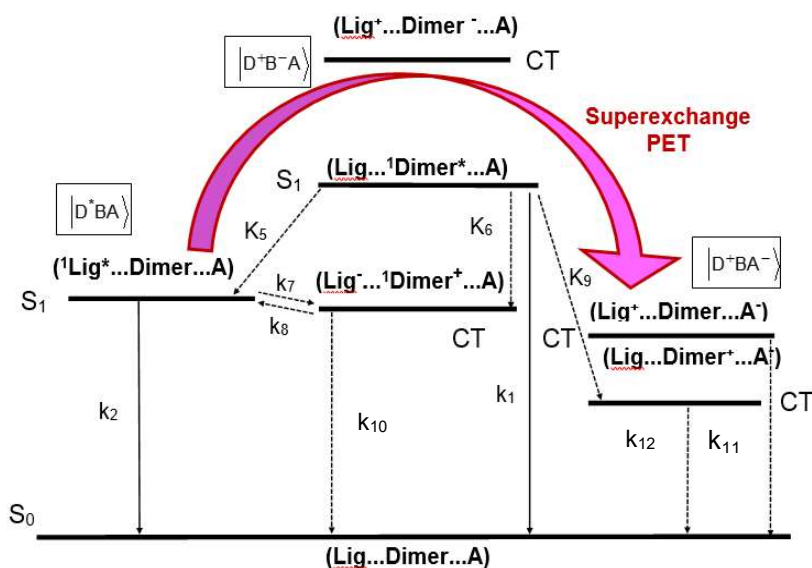

Figure 14. Schematic energy level diagram of excited states for triads III and IV containing electron acceptors Q or Pim. Indicated are rate constants of the following pathways: k_1, fluorescence and non-radiative decay of the dimer (ZnOEP)$_2$Ph; k_2, fluorescence and non-radiative decay of the extra-ligand $H_2P(m^\wedge Pyr)_2$-(iso-PrPh)$_2$ (low effective intersystem crossing $S_1 \leadsto T_1$ is not shown); k_5, singlet-singlet EM (ZnOEP)$_2$Ph → extra-ligand; k_6, photoinduced PET (ZnOEP)$_2$Ph $\leadsto$ extra-ligand leading to the singlet radical ion pair state CT formation; k_7, photoinduced hole transfer from the extra-ligand to the dimer leading to the singlet radical ion pair state formation; k_8, thermally activated charge recombination from the singlet radical ion pair state to the extra-ligand locally excited singlet state; k_9, charge recombination from the triplet state of the radical ion pair to the locally excited triplet state of the extra-ligand; k_{10}, charge recombination from the singlet state of the radical ion pair to the ground state; k_{11}, non-radiative intersystem crossing $T_1 \leadsto S_0$ from the extra-ligand locally excited state to the ground state.

Conclusions

In summary, we showed that the combination of the modern fs/ps time-resolved spectroscopic approach and theoretical modelling gives a deeper insight into the complexity and efficiency of the photoinduced electron transfer among other pathways of the non-radiative relaxation of excited states in multicomponent nano-assemblies containing porphyrin macrocycles. Some basic and relatively rare PET events were observed and analyzed using theoretical calculations.

We have found that both S_1 and T_1 states of *meso*-nitro-phenyl octaethylporphyrins and their chemical dimers are quenched relative to the corresponding states of the parent compounds without nitro groups. The direct PET processes are responsible for the observed fluorescence quenching, and PET rate constants are in a reasonable agreement with the predictions of Marcus theory. The population of the locally excited low-lying T_1 state may take place from the upper-lying triplet or singlet CT states. With respect to other nitroporphyrins, our results demonstrate clearly that steric hindrance effects and the nature of the linkage between D and A influence essentially on the efficiency and the mechanism of PET. For the *meso*-nitrophenyl substituted dimer OEP-Ph-OEP-Ph(o-NO$_2$), the competition between PET and energy migration manifests itself in PET reduced rate constant relative to that for the corresponding monomer OEP-Ph(o-NO$_2$).

For the *meso*-phenyl coupled chemical dimer (ZnOEP)$_2$Ph containing the electron acceptor (*para*-benzoquinone) covalently linked via *meso*-phenyl ring to the porphyrin macrocycle, PET rate constant is smaller essentially compared to that found for monomeric ZnP-Q compounds with the same geometry. The reason of that is explained by the competition between the non-radiative energy migration among dimer subunits and PET to quinone from one half of the dimer.

In the case of the self-assembled triad (ZnOEP)$_2$Ph⊗ H$_2$P(m^Pyr)$_2$-(iso-PrPh)$_2$ it was evidently shown that the fluorescence of the dimer (ZnOEP)$_2$Ph is quenched by two competing processes, namely PET and energy migration to the extra-ligand. PET realization becomes the main relaxation process upon the solvent polarity rise. In the triad containing the fluorinated free base porphyrin (a strong electron acceptor) the charge transfer state is considerably lower in energy than the excited states of the dimer and ligand, thus the efficient PET faster than 1 ps occurs. This PET cannot be slowed down remarkably at low temperature (T=164 K), thus mimicking low temperature PET in natural photosystems. In both triads the decay to the ground state is realized via the free base triplet state population.

The above results provided a good background for the investigation of the relaxation dynamics in self-assembled porphyrin triads, containing the main biomimetic components, Zn-porphyrin dimer, porphyrin free base and electron acceptor (quinone or pyromellitimide). A strong quenching of the dimer S_1 state in these triads originates from both energy and sequential PET processes from the dimer to the extra-ligand which are faster with respect to a slower PET from the dimer to covalently linked acceptors (Q or Pim). A non-radiative deactivation of the extra-ligand S_1 state (in a picosecond time scale) is due to competing processes, long-range superexchange ET to acceptor, mediated by a bridge (the dimer), and photoinduced hole transfer from the extra-ligand to the dimer. The subsequent PET steps dimer→monomer→*A* taking place in the triads, mimics the sequence of primary electron transfer reactions in natural photosynthetic reaction centers.

The issues raised herein seem to be of interest in research concerning the development and studies of synthetic multiporphyrin arrays modelling light-harvesting and charge-transfer phenomena *in vivo* as well as for the rational design and application of multimolecular devices for nanophotonics and nanoelectronics.

References

1. Bryant D.A., Hunter C.N., Warren M.J. *Biol Chem.* **2020**, *295*, 6888–6925.
2. Rehhagen C., Argüello Cordero M.A., Kamounah F.S., Deneva V., Angelov I., Krupp M., Svenningsen S.W., Pittelkow M., Lochbrunner S., Antonov L. *J. Am. Chem. Soc.* **2024**, *146*, 2043–2053.
3. Hutskalov I., Linden A., Ćorić I. *J. Am. Chem. Soc.* **2023**, *145*, 8291–8298.
4. Koifman O.I., Ageeva T.A., Beletskaya I.P., Averin A.D., Yakushev A.A., Tomilova L.G.,.Dubinina T.V., Tsivadze A.Yu., Gorbunova Yu.G., Martynov A.G., Konarev D.V., Khasanov S.S., Lyubovskaya R.N., Lomova T.N., Korolev V.V., Zenkevich E.I., Blaudeck T., von Borczyskowski Ch., Zahn D.R.T., Mironov A.F., Bragina N.A., Ezhov A.V., Zhdanova K.A., Stuzhin P.A., Pakhomov G.L., Rusakova N.V., Semenishyn N.N., Smola S.S., Parfenyuk V.I., Vashurin A.S., Makarov S.V., Dereven'kov I.A., Mamardashvili N.Zh., Kurtikyan T.S., Martirosyan G.G., Burmistrov V.A., Aleksandriiskii V.V., Novikov I.V., Pritmov D.A., Grin M.A., Suvorov N.V., Tsigankov A.A., Fedorov A.Yu., Kuzmina N.S., Nyuchev A.V., Otvagin V.F., Kustov A.V., Belykh D.V., Berezin D.B., Solovieva A.B., Timashev P.S., Milaeva E.R., Gracheva Yu.A., Dodokhova M.A., Safronenko A.V., Shpakovsky D.B., Syrbu S.A., Gubarev Yu.A., Kiselev A.N., Koifman M.O., Lebedeva N.Sh., Yurina E.S. Macroheterocyclic Compounds – a Key Building Block in New Functional Materials and Molecular Devices. *Macroheterocycles* **2020**, *13*, 311–467.
5. Jing H., Rong J., Taniguchi M., Lindsey J.S. *Coord. Chem. Rev.* **2022**, *456*, 214278.
6. Koifman O.I., Ageeva T.A., Kuzmina N.S., Otvagin V.F., Nyuchev A.V., Fedorov A.Yu., Belykh D.V., Lebedeva N.Sh., Yurina E.S., Syrbu S.A., Koifman M.O., Gubarev Y.A., Bunin D.A., Gorbunova Yu.G., Martynov A.G., Tsivadze A.Yu., Dudkin S.V., Lyubimtsev A.V., Maiorova L.A., Kishalova M.V., Petrova M.V., Sheinin V.B., Tyurin V.S., Zamilatskov I.A., Zenkevich E.I., Morshnev P.K., Berezin D.B., Drondel E.A., Kustov A.V., Pogorilyy V.A., Noev A.N., Eshtukova-Shcheglova E.A., Plotnikova E.A., Plyutinskaya A.D., Morozova N.B., Pankratov A.A., Grin M.A., Abramova O.B., Kozlovtseva E.A., Drozhzhina V.V., Filonenko E.V., Kaprin A.D., Ryabova A.V., Pominova D.V., Romanishkin I.D., Makarov V.I., Loschenov V.B., Zhdanova K.A., Ivantsova A.V., Bortnevskaya Yu.S., Bragina N.A., Solovieva A.B., Kuryanova A.S., Timashev

P.S. Synthesis Strategy of Tetrapyrrolic Photosensitzers for Their Practical Application in Photodynamic Therapy. *Macroheterocycles* **2022**, *15*, 207–302.

7. Francesca S., Wennink J.W.H., Mäkinen P.I., Holappa L.P., Trohopoulus P.N., Ylä-Herttuala S., van Nostrum C., de la Escosura A., Torres T. *J. Mater. Chem. B* **2020**, *8*, 282–289.

8. Drain C.M., Varotto A., Radivojevic I. *Chem Rev.* **2009**, *109*, 1630–1658.

9. *Multiporphyrin Arrays: Fundamentals and Applications* (Kim D., Ed.), Singapore: Pan Stanford Publ. Pte. Ltd., **2012**. 775 p.

10. Zenkevich E.I., von Borczyskowski Ch. Multiporphyrin Self-Assembled Arrays in Solutions and Films: Thermodynamics, Spectroscopy and Photochemistry. In: *Handbook of Polyelectrolytes and Their Applications, Vol. 2* (Tripathy S.K., Kumar J., Nalwa H.S., Eds.) USA: American Scientific Publishers, **2002**. Ch. 11, 301–348.

11. Zenkevich E.I., von Borczyskowski Ch.W. Formation Principles and Excited States Relaxation in Self-Assembled Complexes: Multiporphyrin Arrays and "Semiconductor CdSe/ZnS Quantum Dot-Porphyrin" Nanocomposites. In: *Handbook of Porphyrin Science with Application to Chemistry, Physics, Materials Science, Engineering, Biology and Medicine. Volume 22 – Biophysical and Physicochemical Studies of Tetrapyrroles* (Kadish K., Smith K.M., Guilard R., Eds.). Singapore: World Scientific Publishing Co. Pte. Ltd., **2012**. Ch. 104, p. 68–159

12. Enakieva Y.Y., Zhigileva E.A., Fitch A.N., Chernyshev V.V., Stenina I.A., Yaroslavtsev A.B., Sinelshchikova A.A., Kovalenko K.A., Gorbunova Y.G., Tsivadze A.Yu. *Dalton Trans.* **2021**, *50*, 6549–6560.

13. Maiorova L.A., Kobayashi N., Zyablov S.V., Bykov V.A., Nesterov S.I., Kozlov A.V., Devillers C.H., Zavyalov A.V., Alexandriysky V.V., Orena M., Koifman O.I. *Langmuir* **2018**, *34*, 9322–9329.

14. Urbani M., Grätzel M., Nazeeruddin M.K., Torres T. *Chem. Rev.* **2014**, *114*, 12330–12396.

15. Zenkevich E., von Borczyskowski Ch. Surface Photochemistry of Quantum Dot-Porphyrin Nanoassemblies for Singlet Oxygen Generation. In: *Photoinduced Processes at Surfaces and in Nanomaterials, ACS Symposium Series, Vol. 1196* (Kilin D., Ed.). Washington: American Chemical Society, **2015**. Ch. 12, p. 235–272.

16. Liu Q., Sun O., Shen J., Zhang Y., Li H., Yu S., Chen Y., Li X., Jiang J. *J. Porphyrins Phthalocyanines* **2023**, *27*, 1119–1125.

17. Li J., Lu Z., Guo Y., Fang J., Wang A., Feng Y., Zhang Y., Zhu J., Zhao Z., Cheng X., Shi H. *ACS Nano* **2023**, *17*, 25147−25156.

18. Roy P.P., Kundu S., Valdiviezo J., Bullard G., Fletcher J.T., Liu R., Yang S.J., Zhang P., Beratan D.N., Therien M.J., Makri N., Fleming G.R. *J. Am. Chem. Soc.* **2022**, *144*, 6298–6310.

19. Pochan D., Scherman O. *Chem. Rev.* **2021**, *121*, 13699–13700.

20. Förster T. *Modern Quantum Chemistry* (Sinanoglu O., Ed.). New York: Academic Press, **1965**.

21. Agranovich V.M., Galanin M.D. *Electronic Excitation Energy Transfer in Condensed Matter*. Amsterdam, New York: North-Holland Pub. Co. **1982**.

22. Marcus R.A. *Rev. Modern Phys.* **1993**, *65*, 599–610.

23. Uno T., Koga M., Sotome H., Miyasaka H., Tamai N., Kobayashi Y. *J. Phys. Chem. Lett.* **2018**, *9*, 7098−7104.

24. Lawrence J.E., Mannouch J.R., Richardson J.O. *J. Phys. Chem. Lett.* **2024**, *15*, 707–716.

25. Wasielewski M.R. *Chem. Rev.* **1992**, *92*, 435–461.

26. Kuciauskas D., Lin S., Seely G.R., Moore A.L., Moore T.A., Gust D., Drovetskaya T., Reed C.A., Boyd P.D.W. *J. Phys. Chem.* **1996**, *100*, 15926–15932.

27. Zenkevich E.I., Shulga A.M., Bachilo S.M., Rempel U., von Richthofen J., von Borczyskowski Ch. *J. Lumin.* **1998**, *76–77*, 354–358.

28. Bachilo S., Willert A., Rempel U., Shulga A.M., Zenkevich E.I., von Borczyskowski Ch. *J. Photochem. Photobiol. A: Chemistry* **1999**, *126*, 99–112.

29. Aoki T., Sakai H., Ohkubo K., Sakanoue T., Takenobu T., Fukuzumi S., Hasobe T. *Chem. Sci.* **2015**, *6*, 1498–1509.

30. Bancroft L., Zhang J., Harvey S.M., Krzyaniak M.D., Zhang P., Schaller R.D., Beratan D.N., Young R.M., Wasielewski M.R. *J. Phys. Chem. A* **2021**, *125*, 825–834

31. Sissaoui J., Efimov A., Kumpulainen T., Vauthey E. *J. Phys. Chem. B* **2022**, *126*, 4723–4730.

32. Bichan N.G., Ovchenkova E.N., Mozgova V.A., Ksenofontov A.A., Kudryakova N.O., Shelaev I.V., Gostev F.E., Lomova T.N. *Molecules* **2022**, *27*, 8900.

33. Washburn S., Kaswan R.R., Shaikh S., Moss A., D'Souza F., Wang H. *J. Phys. Chem. A* **2023**, *127*, 9040–9051.

34. Kim T., Feng Y., O'Connor J.P., Stoddart J.F., Young R.M., Wasielewski M.R. *J. Am. Chem. Soc.* **2023**, *145*, 8389–8400.

35. Chen Z., Deng J.-R., Hou S., Bian X., Swett J.L., Wu Q., Baugh J., Bogani L., Briggs G.A.D., Mol J.A., Lambert C.J., Anderson H.L., Thomas J.O. *J. Am. Chem. Soc.* **2023**, *145*, 15265−15274.

36. Knyukshto V., Zenkevich E., Sagun E., Shulga A., Bachilo S. *Chem. Phys. Lett.* **1998**, *297*, 97–108.

37. Knyukshto V., Zenkevich E., Sagun E., Shulga A., Bachilo S. *J. Fluoresc.* **2000**, *10*, 55–68.

38. Knyukshto V.N., Shulga A.M., Sagun E.I., Zenkevich E.I. *Opt. Spectrosc.* **2002**, *92*, 59–68.

39. Chernook A.V., Shulga A.M., Zenkevich E.I., Rempel U., von Borczyskowski Ch. *J. Phys. Chem.* **1996**, *100*, 1918–1926.

40. Osuka A., Tanabe N., Nakajima S., Maruyama K. *J. Chem. Soc. Perkin Trans.* **1996**, *2*, 199–203.

41. Sessler J.L., Capuano V.L., Harriman A. *J. Am. Chem. Soc.* **1993**, *115*, 4618–4628.

42. Osuka A., Marumo S., Mataga N., Taniguchi S., Okada T., Yamazaki I., Nishimura Y., Ohno T., Nozaki K. *J. Am. Chem. Soc.* **1996**, *118*, 155–168.

43. Zenkevich E.I., von Borczyskowski Ch. Photoinduced Relaxation Processes in Self-Assembled Nanostructures: Multiporphyrin Complexes and Composites "CdSe/ZnS Quantum Dot-Porphyrin". In: *Multiporphyrin Arrays: Fundamentals and Applications* (Kim D., Ed.) Singapore: Pan Stanford Publishing Pte. Ltd., **2012**. Ch. 5, 217–288.

44. Knyukshto V., Zenkevich E., Sagun E., Shulga A., Bachilo S. *Chem. Phys. Lett.* **1998**, *297*, 97–108.

45. Sagun E.I., Zenkevich E.I., Knyukshto V.N., Panarin A.Yu., Semeikin A.S., Lyubimova T.V. *Opt. Spetrosc.* **2012**, *113*, 388–400.

46. Sagun E.I., Zenkevich E.I. *Opt. Spectrosc.* **2013**, *115*, 727–738.

47. Gorski A., Knyukshto V., Zenkevich E., Starukhin A., Kijak M., Solarski J., Semeikin A., Lyubimova T. *J. Photochem. Photobiol. A: Chemistry* **2018**, *354*, 101–111.

48. Gorski A., Kijak M., Zenkevich E., Knyukshto V., Starukhin A., Semeikin A., Lyubimova T., Waluk J. *J. Phys. Chem. A* **2020**, *124*, 8144–8158.

49. Pukhovskaya S.G., Guseva L.S., Semeikin A.S., Kuvshinova E.M., Golubchikov O.A. *Zh. Neorg. Khim.* **2005**, *50*, 635–639.

50. Senge M.O., Medforth C.J., Forsyth T.P., Lee D.A., Olmstead M.M., Jentzen W., Pandey R.K., Shelnutt J.A., Smith K.M. *Inorg. Chem.* **1997**, *36*, 1149–1163.

51. Barkigia K.M., Nurco D.J., Renner M.W., Melamed D., Smith K.M., Fajer J. *J. Phys. Chem. B* **1998**, *102*, 322–326.

52. Shi Z., Franco R., Haddad R., Shelnutt J.A., Ferreira G.C. *Biochemistry* **2006**, *45*, 2904–2912.

53. Medforth C.J., Berget P.E., Fettinger J.C., Smith K.M., Shelnutt J.A. *J. Porphyrins Phthalocyanines* **2016**, *20*, 307–317.

54. Retsek J.L., Medforth C.J., Nurco D.J., Gentemann S., Chirvony V.S., Smith K.M., Holten D. *J. Phys. Chem. B* **2001**, *105*, 6396–6411.

55. Rozas I., Senge M.O. *Future Med. Chem.* **2016**, *8*, 609–612.

56. Fraser D.D., Bolton J.R. *J. Phys. Chem.* **1994**, *98*, 1626–1633.

57. Sessler J.L., Johnson M.R., Lin T.-Y. *Tetrahedron* **1989**, *45*, 4767–4784.

58. Knyukshto V., Zenkevich E., Sagun E., Shulga A., Bachilo S. *Chem. Phys. Lett.* **1999**, *304*, 155–166.

59. Sagun E.I., Zenkevich E.I., Knyukshto V.N., Tikhomirov S.A., Shulga A.M. *Opt. Spectrosc.* **2004**, *96*, 388–402.

60. Sagun E.I., Zenkevich E.I., Knyukshto V.N. Charge-Transfer Interactions in Sterically Hindered Porphyrins. In: *Spectroscopy and Luminescence of Molecular Systems* (Voropay E.S., Solovyev K.N., Umreiko D.S., Eds.). Minsk, **2002**. p. 133–150 [В кн.: *Спектроскопия и люминесценция молекулярных систем* (Воропай Е.С., Соловьекв К.Н., Умрейко Д.С., ред.). Минск: БГУ, **2002**. с. 133–155], ISBN 985-445-811-3.

61. Kavarnos G.J. *Fundamentals of Photoinduced Electron Transfer*. New-York: VCH Publishers, Inc., **1993**. Ch. 6, p. 287–342.

62. Avilov I.V., Zenkevich E.I., Sagun E.I., Shulga A.M., Filatov I. V. *Opt. Spektrosk.* **2003**, *95*, 696–706.

63. Murrov S.L., Carmichael I., Hug G.L. *Handbook of Photochemistry*. New-York-Basel-Hong Kong: Marcel Deccer, Inc. **1993**. p. 269–278.

64. Gust D., Moore T.A., Moore A.L., Kang H.K., De Graziano J.M., Liddell P.A., Seely G.R. *J. Phys. Chem.* **1993**, *97*, 13637–13642.

65. Kavarnos G.J., Turro N.J. *Chem. Rev.* **1986**, *86,* 401–449.

66. Johnson D.J., Niemczyk M.P., Minsek D.W., Wiererrechy G.P., Svec W.A., Gaines III G.L., Wasielewski M.R. *J. Am. Chem. Soc.* **1993**, *115*, 5692–5701.

67. Liu J., Bolton J.R. *J. Phys. Chem.* **1992**, *96,* 1718–1725.

68. Asahi T., Ohkohchi M., Matsusaka R., Mataga N., Zang R.P., Osuka A., Maruyama K. *J. Am. Chem. Soc.* **1993**, *115*, 5665–5674.

69. Zenkevich E.I. *Russ. J. Gen. Chem.* **2019**, *89*, 2650–2681.

70. Zenkevich E.I., Larkina E.A., Konovalova N.V., Stupak A.P. *Macroheterocycles* **2019**, *12*, 47–57.

71. Zenkevich E.I. *Macroheterocycles* **2016**, *9*, 121–140.

72. Zenkevich E.I., von Borczyskowski C. Shulga A.M., Bachilo S.M. Rempel U., Willert A. *Chem. Phys.* **2002**, *275*, 185–209.

73. Zenkevich E.I., von Borczyskowski C., Shulga A.M. *J. Porphyrins Phthalocyanines* **2003**, *7*, 731–754.

74. Zenkevich E.I., Willert A., Bachilo S.M., Rempel U., Kilin D.S., Shulga A.M., von Borczyskowski Ch. *Mater. Sci. Eng., C* **2001**, *18*, No 1–2, 99–111.

75. Zenkevich E.I., Kilin D., von Borczyskowski C., Zahn D.R.T. *Macroheterocycles* **2020**, *13*, 130–141.

76. Gust D., Moore T.A., Moore A.L., Leggett L., Lin S., DeGraziano J.M., Hermant R.M., Nicodem D., Craig P., Seely G.R., Nieman R.A. *J. Phys. Chem.* **1993**, *97*, 7926–7931.

77. Dorfman K.E., Zhang Y., Mukamel S. *Proc. Natl. Acad. Sci. USA* **2016**, *113*, 10001–10006.

78. Fleming G.R., Martin G.L., Breton J. *Nature* **1988**, *333*, 190–192.

79. Wasielewski M.R., Johnson D.G., Svec W.A., Kersey, K.M., Minsek D.W. *J. Am. Chem. Soc.* **1988**, *110*, 7219–7221.

80. Felton R. In: *The Porphyrins, Vol. V* (Dolphin D., Ed.) New York: Acad. Press, **1978**. p. 53.

81. Majranowski V.G. In: *Porphyrins: Spectroscopy, Photochemistry, Applications* (Enikolopyan N.S., Ed.) Moscow, **1987**, p. 127–181 [Майрановский В.Г. В кн.: *Порфирины: спектроскопия, фотохимия, применение* (Ениколопян Н.С., ред.). М.: Наука, **1987**. с. 127–181].

82. Osuka A., Yamada H., Maruyama K., Mataga N., Asahi T., Ohkoshi M., Okada T., Yamazaki I., Nishimura Y. *J. Am. Chem. Soc.* **1993**, *115*, 9439–9447.

83. Rempel U., Meyer S., von Maltzan B., von Borczyskowski C. *J. Lumin.* **1998**, *78*, 97–102.

84. Davis W., Wasielewski M.R., Ratner M., Mujica V., Nitzan A. *J. Phys. Chem.* **1997**, *101*, 6158–6164.

85. Bixon M., Jortner J., Michel-Beyerle M.E. *Chem. Phys.* **1995**, *197*, 389–404.

86. Kilin D., Kleinekathofer U., Schreiber M. *J. Phys. Chem. A* **2000**, *104*, 5421.